August 2021

Optimal Pacing of Cyclists in a Time Trial Based on Experimentally Calibrated Models of Fatigue and Recovery

Faraz Ashtiani
Clemson University, faraz.ashtiani@gmail.com

Optimal Pacing of cyclists in a Time Trial Based on Experimentally Calibrated Models of Fatigue and Recovery

---

A Dissertation
Presented to
the Graduate School of
Clemson University

In Partial Fulfillment
of the Requirements for the Degree
Doctor of Philosophy
Mechanical Engineering

---

by
Faraz Ashtiani
August 2021

Accepted by:
Dr. Ardalan Vahidi, Committee Chair
Dr. Gregory Mocko
Dr. Phanindra Tallapragada
Dr. John Wagner
Dr. Randolph Hutchison

Abstract

This dissertation pushes on the boundaries of improving human performance through individualized models of fatigue and recovery, and optimization of human physical effort. To that end, it focuses on professional cycling and optimal pacing of cyclists on hilly terrains during individual and team time trial competitions. Cycling is an example of physical activity that provides nice interfaces for real-time performance measurement through inexpensive power meters, and for providing real-time feedback via a mobile displays such as smartphones. These features enable implementing a real-time control system that provides the optimal strategy to cyclists during a race.

There has been a lot of work on understanding the physiological concepts behind cyclists' performance. The concepts of Critical Power (CP) and Anaerobic Work Capacity (AWC) have been discussed often in recent cycling performance related articles. CP is a power that can be maintained by a cyclist for a long time; meaning pedaling at or below this limit, can be continued until the nutrients end in the cyclist's body. However, there is a limited source of energy for generating power above CP. This limited energy source is AWC. After burning energy from this tank, a cyclist can recover some by pedaling below CP.

In this dissertation, we utilize the concepts of CP and AWC to mathematically model muscle fatigue and recovery of cyclists. We use experimental data from six

human subjects to validate and calibrate our proposed dynamic models. The recovery of burned energy from AWC has a slower rate than expending it. The proposed models capture this difference for each individual subject. In addition to the anaerobic energy dynamics, maximum power generation of cyclists is another limiting factor on their performance. We show that the maximum power is a function of both a cyclist's remaining anaerobic energy and the bicycle's speed.

These models are employed to formulate the pacing strategy of a cyclist during a time trial as an optimal control problem. Via necessary conditions of Pontryagin Minimum Principle (PMP), we show that in a time trial, the cyclist's optimal power is limited to only four modes of maximal effort, no effort, pedaling at critical power, or pedaling at constant speed. To determine when to switch between these four modes, we resort to numerical solution via dynamic programming. One of the subjects is then simulated on four courses including that of the 2019 Duathlon National Championship in Greenville, SC. The simulation results show reduced time over experimental results of the self-paced subject who is a competitive amateur cyclist.

Moreover, we expand our optimal control formulation from an individual time trial to a Team-Time-Trial (TTT) competition. In a TTT cyclists on each team follow each other closely. This enables the trailing cyclists to benefit from a rather significant reduction in drag force. Through a case study for a two-cyclist team, we show that the distance between the cyclists does not need to be variable and can be set at the minimum safe gap. We then use this observation to formulate the problem for an n-cyclist team. We propose a Mixed-Integer Non-Linear Programming (MI-NLP) formulation to determine the optimal positioning strategy in addition to optimal power and velocity trajectories for a three-cyclist team. The results show improved travel time compared to a baseline strategy that is popular among cycling teams.

The results from this work highlight the potential of mathematical optimization of athletes' performance both prior and during a race. The proposed models of fatigue and recovery can help athletes better understand their abilities at their limits. To prepare for a race, cyclists can practice over the simulated elevation profile of the race on a stationary bicycle with the optimal strategies we proposed. Additionally, if allowed by the rules of a specific competition, a cyclist can be provided with real-time race strategies. There is also the potential for integrating the proposed algorithms into the available commercial smart stationary bicycles for improving well-being and training of the general public.

Dedication

With all my heart, I dedicate this dissertation to my beloved parents Mohammadreza and Nahid, and my dear brother Farshid. All my past, present, and future accomplishments in life are because of your support, sacrifices, and love.

Also, I would like to dedicate this dissertation to my wonderful advisor Prof. Ardalan Vahidi. Thank you for your unconditional support, mentorship, and kindness, and thank you for believing in me and always motivating me to be the best version of myself.

Acknowledgments

First, I want to thank all of our fantastic human subjects who agreed to perform a series of extremely challenging experiments and helped this project progress.

Second, I want to thank faculty members Dr. Rnadolph Hutchison and Dr. Gregory Mocko whose advice, guidance, and suggestions were very substantial for the progress of the project. I also, would like to thank the former PhD student who collaborated closely with me on this project, my dear friend, Dr. Vijay Sarthy M Sreedhara. Without Vijay's hard work and insights, this dissertation would be impossible. Additionally, I want to thank Furman University students Frank Lara, Mason Coppi, Nicholas Hayden, Lee Shearer, Brendan Rhim, Alec Whyte, and Jake Ogden for their contribution in data collection from recruited human subjects.

I would like to thank my lab mates Dr. Alireza Fayazi, Dr. Ausin Dollar, Shahab Karimi, Tyler Ard, and Angshuman Goswamy for their support and friendship during my PhD journey. Working with these people made these past five years joyful.

Last but not least, I would like to thank the distinguished faculty members Dr. John Wagner, Dr. Phanindra Tallapragada, Dr. Gregory Mocko, and Dr. Randolph Hutchison who kindly accepted my invitation to be a member of my dissertation committee.

Table of Contents

List of Tables

List of Figures

Chapter 1

Introduction

Optimization of human performance by accurately modeling fatigue has challenged athletes, coaches, and scientists. The rise in popularity of wearable sensors in physical activity tracking presents opportunities for modeling and optimizing performance as they alleviate the need for expensive laboratory equipment. Understanding fatigue dynamics can potentially help athletes train in a more efficient way and perform at their peak. Moreover, it can provide useful information to further enhance the performance of an athlete during a physical exercise. Fatigue due to prolonged exercise is defined as a decline in muscle performance which accompanies a sensation of tiredness [5, 6]. Therefore, during physical exercise, fatigue prevents athletes from producing the required power.

Cycling is an example of physical exercise that enables a systematic performance optimization given the known dynamics of a bicycle's movement. There are several types of commercial sensors, such as power, heart rate, cadence, and muscle oxygenation, that can be mounted on a bicycle or worn by a cyclist for monitoring the cyclist's performance. Obtaining data from these sensors can help in developing individualized optimal strategy for a race. Figure 1.1 illustrates a cyclist pedaling

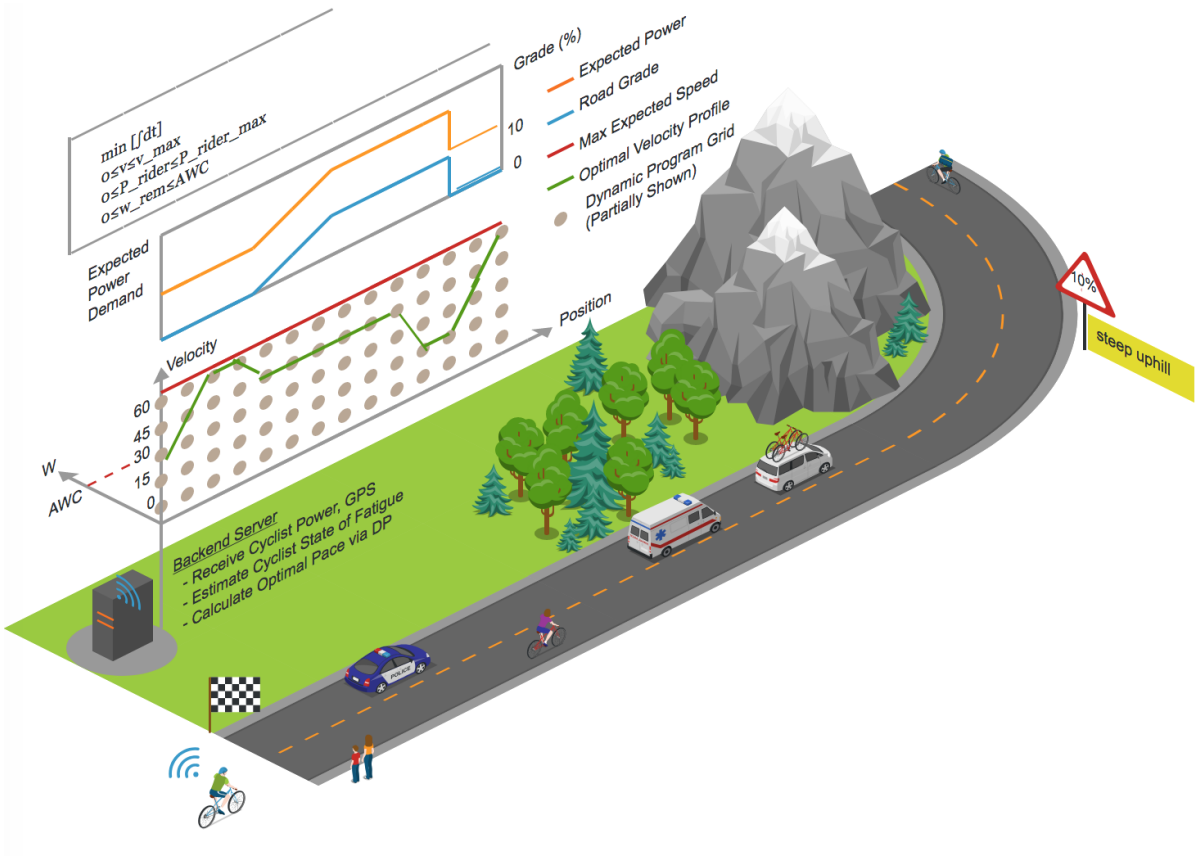

Figure 1.1: An illustration of optimal pacing of a cyclist using upcoming elevation data, a dynamic model of cyclist fatigue and recovery, and a model of bicycle longitudinal dynamics. The illustration also shows a dynamic programming grid on two states of velocity and anaerobic energy for planning the optimal velocity or power. The optimal power is communicated and displayed to the cyclist in real-time. Drawn in https://www.icograms.com.

in a time trial on a mountain course. Even seasoned cyclists may find it challenging to pace themselves in such a course. By over exerting themselves too early or too late, they may not achieve their maximum potential. We hypothesize that cyclists can finish a time trial faster if they plan in advance in consideration of their state of fatigue and upcoming road elevation. The pacing strategy can be formalized as an optimal control problem which requires dynamic models of fatigue and recovery and maximal power capacity of a cyclist as a function of their fatigue levels. While former members of our team had attempted optimal pacing based on a dynamic model of muscle fatigue and recovery in [7] and [8], such lumped muscle models were complex and hard to experimentally verify and calibrate.

Several studies such as [9, 10, 11] have investigated fatigue in cycling and developed models for it based on the expenditure of anaerobic energy. Only a few studies investigate the recovery dynamics of this anaerobic energy [12]. Alternatively, one can consider fatigue as running out of Anaerobic Work Capacity (AWC) which is a limited tank of anaerobic energy, and recovery as reconstitution of AWC when pedaling below a Critical Power (CP). Such a model can be more easily verified and calibrated in laboratory experiments as our recent work in [13, 14, 15] shows. In fact, a model based on anaerobic energy expenditure has been used in [16] to optimize a 5 km cycling time-trial. However, a model for recovery was not considered in [16]. In order to hypothesize dynamic models of fatigue and recovery, we first need to review the current models presented in literature.

1.1 Literature Review

1.1.1 Fatigue Definition and Mechanism

Several studies have investigated fatigue, which has led to its many definitions. For example, in [17] authors define fatigue as a reduction in maximal capacity to generate force or power during exercise. Whereas, fatigue is defined as inability to produce the desired force or power resulting in impaired performance in [18] and [19]. The point of occurrence of fatigue is defined as the moment at which a drop from the desired power level is observed, which is also time-to-exhaustion, thus making both terms indistinguishable [20]. To address this, in [21] and [22] fatigue is defined as a continuous process altering the neuromuscular functional state resulting in exhaustion and exercise termination. In general, there are two sources of fatigue: central fatigue and peripheral fatigue [23]. Central fatigue is defined as the failure of the Central Nervous System (CNS) in sending necessary commands to muscles to operate [24]. This factor is essentially important in high-intensity exercise [25]. Peripheral fatigue is caused at the muscle level. It can be induced because of the neuromuscular failure in muscles to comprehend and perform the commands coming from CNS, and deficiency of vital substances [25].

The above mentioned studies illustrate the difficulty involved in arriving at a global definition of fatigue. The mechanism of fatigue leading to exhaustion are different for cycling, running, swimming, etc [26]. As we previously presented in [13], we define muscle fatigue and recovery in cycling as follows:

- *Fatigue*: Expending energy from anaerobic metabolic systems by pedaling above a critical power which results in a decrease of maximum power generation ability.
- *Recovery*: Recovering energy from anaerobic metabolic systems by pedaling be-

low the critical power which results in an increase of maximum power generation ability.

1.1.2 Muscle Fatigue Measurement and Modeling

Measuring the effect of central fatigue on muscle performance is a challenge since the the matter is highly subjective [27]. Most research efforts to objectively measure central fatigue are focused on measurement of Maximum Voluntary Contraction (MVC) [28, 29, 30]. In voluntary contraction of a muscle, the generated force is proportional to the muscle electrical activation [31]. A standard way of measuring muscle activity is via Electromyography (EMG) tests. During the test the amount of electric potential produced in muscles can be measured. Although studies such as [32] and [33] have shown the accuracy of EMG tests in measuring maximal and submaximal voluntary contractions, there is evidence of underestimating muscle activation at high force levels [23]. Therefore, to point to the goal of the current study, EMG cannot provide accurate data for modeling a cyclist's fatigue and recovery.

In addition to central fatigue there are several sites for peripheral fatigue. To get a better understanding of fatigue at muscle level, we should focus on muscle metabolic system. Like all of the natural processes in the world, muscle contraction needs a source of energy to be executed. The fuel that provides this energy is adenosine triphosphate (ATP). When one phosphate radical detaches from ATP, more than 7300 calories of energy are released to supply the energy needed for muscle contraction [1]. After this detachement, ATP converts to adenosine diphosphate (ADP). When a human muscle is fully rested, the amount of available ATP is sufficient to sustain maximal muscle power for only about 3 seconds, even in trained athletes [1]. Therefore, for any physical activity that lasts more than a few seconds, it is essential

Table 1.1: Comparison between three metabolic systems that provide ATP for muscle contraction [1].

Metabolic system	Moles of ATP/min	Endurance time
Phosphagen system	4	8-10 seconds
Glycogen-lactic acid system	2.5	1.3-1.6 minutes
Aerobic	1	Unlimited (as long as nutrients last)

that new ATP be formed continuously.

There are three metabolic systems which provide the needed ATP: Aerobic system , Glycogen-lactic acid system and Phosphagen system. Table 1.1 compares the three systems, in terms of moles of ATP generation per minute and endurance time at maximal rates of power generation. Utilization of these systems during physical activity is based on the intensity of the activity.

Cycling can fall in all categories above depending on the intensity of the exercise. Many people cycle for fun and get around cities. In this case they may only use their aerobic system which provides them with low amount of power which they can hold for a very long time. However, during high intensity cycling such as in a time trial, the human body will use the other two sources besides the aerobic system to provide enough energy for muscle contraction. This is important when designing mathematical models that describe muscle power generation in cycling. Later on, we discuss a method to define a power limit below which the cyclists use their aerobic metabolic system that allows them to hold their power for long periods of time. However, there is limited energy to pedal above this power limit.

During aerobic exercise, muscles utilize the aerobic metabolic system to produce ATP. Oxygen plays a vital role in formation of ATP molecules. There are two major methods to measure oxygen during a fatiguing exercise. The first one is measuring the volume of oxygen intake in breathing ($\dot{V}_{O_2}$) [34]. During a physical

exercise, $\dot{V}_{O_2}$ increases to provide the necessary oxygen needed to produce ATP in the muscle as suggested in [35, 36], and modeled in [37]. The experimental procedure to measure $\dot{V}_{O_2}$ requires a number of laboratory equipment that cannot be used by a cyclist during everyday outdoor ride. The second method is directly measuring the amount of oxygenated hemoglobins at the local muscle (muscle oxygenation). When muscles are fully fresh, the percentage of oxygenated hemoglobins among the total number of hemoglobins is at its highest. During a fatiguing exercise, this percentage drops. Several studies show that Near Infrared Spectroscopy (NIRS) is a robust method to measure muscle oxygenation [38, 39, 40]. A few companies currently make wearable devices that enable the cyclists to monitor their muscle oxygenation in real-time [41, 42]. We have shown in [13] a real-time measurement of muscle oxygenation during a set of experiments.

Another fatigue indicator is the amount of lactate produced in the muscle. Maximum Lactate at Steady State ($MLSS$) is the maximum maintainable blood lactate concentration without additional buildup through aerobic exercise [43, 44]. During an anaerobic exercise, the rate of lactate production is higher than its dissipation [45]. As authors in [46] and [47] suggest, the amount of lactate accumulation can provide useful information about the fatigue level of muscles. The high lactate levels at muscle represent a lower ability of the muscle to generate force and power [18, 48, 49]. Traditionally, a common way to measure lactate has been taking blood samples or biopsies during an experiment [50, 51]. These invasive methods are not in any way suitable for real-time measurement and estimation of fatigue. Recently, authors in [52] developed a non-invasive method to measure blood lactate using electromagnetic wave sensors. Commercialization of such non-invasive in-situ measurement techniques will enable researchers to develop mathematical models that represent the relationship between blood lactate level and muscle power/force generation capacity.

1.1.3 Fatigue and Recovery in Cycling

In cycling, it is easier to measure power without elaborate laboratory equipment owing to the development of commercial grade power meters. However, determining exercise intensity using power is not straightforward as a threshold power is needed to classify exercise intensity. As stated in [53] and [54], the Critical Power (CP) can potentially be used to determine exercise intensity. It has been shown that CP is close to the power at which MLSS occurs according to [55, 56, 57]. This means that while pedaling at a power level above CP, a cyclist would expend energy from anaerobic energy sources. On the other hand, pedaling below CP allows the cyclist to partially recover the burned energy using anaerobic metabolic system [55, 56, 57].

The critical power concept was introduced by authors in [58]. They defined CP as the maximum power output that can be maintained indefinitely. In [59] authors showed that there is a limited amount of anaerobic energy for a cyclist to pedal above CP. This "tank" of energy is called *Anaerobic Work Capacity* (AWC). They suggest by pedaling at a certain power level above CP, a cyclist can hold that power for a limited amount of time before he or she runs out of anaerobic energy and cannot pedal above CP. This is known as the *two parameter model*. The relationship between critical power and anaerobic work capacity is often expressed as:

$$P = CP + \frac{AWC}{t_{lim}} \tag{1.1}$$

where P is instantaneous power in Watts, and t_{lim} is time-to-exhaustion in seconds. The experimental protocol designed to calculate CP and AWC in Equation (1.1) requires multiple lab visits for the test subjects according to [10, 11, 60, 61, 62] .

To avoid these multiple lab visits, authors in [63] developed a 3-minute-all-out test (3MT) as in Figure 1.2. In this test, subjects sprint "all-out" for the entire 3

minutes. The value of CP is given by the average power output of the last 30 seconds. The value of AWC is the area between the power curve and CP. This test has been validated in [64] and [65]. Therefore, we can conclude that to calculate the amount of expended anaerobic energy at any point in time, we can simply integrate the power curve above CP.

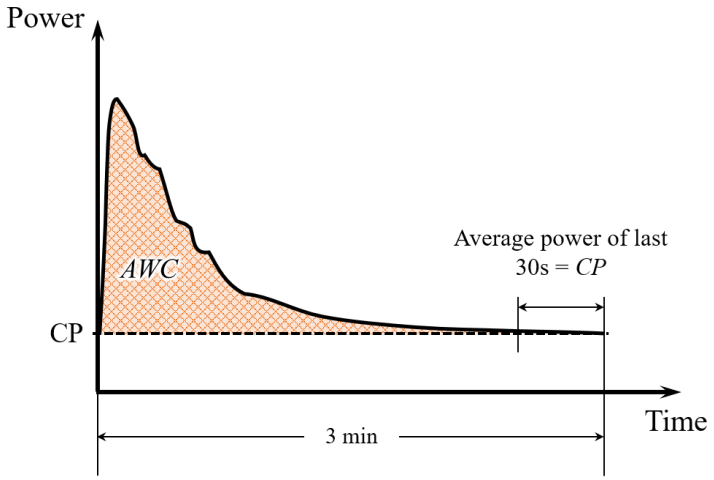

Figure 1.2: The 3-minute-all-out test protocol. The average power at the last 30 seconds of the tests is considered to be CP, and the area between power plot and CP is equivalent to AWC.

On the other hand, recovery happens at a slower rate than fatigue [66, 67]. Authors in [68] propose an exponential model for recovery of anaerobic energy as,

$$W'_{bal} = \int_0^t W'_{exp} e^{\frac{-(t-u)}{\tau_{W'}}} \, du \tag{1.2}$$

where W' is the estimate of AWC from the 3MT test, W'_{bal} is the remaining anaerobic energy at every time, W'_{exp} is the amount of expended energy, $(t-u)$ is the recovery interval duration, and $\tau_{W'}$ is the time constant of reconstitution of W' which is calculated from,

$$\tau_{W'} = 546e^{-0.01D_{CP}+316} \tag{1.3}$$

where D_{CP} is the difference between CP and the average power during the recovery interval. The model in Equation (1.2) has been shown to underestimate the amount of recovered anaerobic energy in [69, 70]. Additionally, in Equation (1.3) $\tau_{W'}$ is calculated as a function of the average power during the recovery interval. However, this average power is not known until the end of the recovery interval. Therefore, the aforementioned model cannot serve as a real-time predictive model of recovery during cycling. In this study, we propose a subject specific recovery model that is predictive and can be used in formulating an optimal control problem for time trial competitions.

1.1.4 Cycling Time Trial

There are a few other studies in which an individual time trial competition is formulated as an optimal control problem such as [7, 16]. The authors in [7] propose dynamic models of fatigue and recovery that are based on the notion of MVC. First, they suggest that the maximum isometric force decays with fatigue according to the relationship below,

$$\frac{dF_{max,iso}(t)}{dt}|_{fatigue} = -kF_{max,iso}(t)\frac{F_{iso}(t)}{MVC} \tag{1.4}$$

where $F_{max,iso}$ is the maximum isometric force generation of a cyclist, k is the model's constant, F_{iso} is the applied isometric force, and MVC is the maximum voluntary contraction of a subject when fully fresh. The authors propose a different model for recovery as,

$$\frac{dF_{max,iso}(t)}{dt}|_{recovery} = R(MVC - F_{max,iso}(t)) \tag{1.5}$$

where R is the model's constant. Combining Equations (1.4) and (1.5) the maximum isometric force generation ability of a cyclist during an exercise can be written as,

$$\frac{dF_{max,iso}(t)}{dt} = -kF_{max,iso}(t)\frac{F_{iso}(t)}{MVC} + R(MVC - F_{max,iso}(t)) \tag{1.6}$$

Knowing the maximum isometric force generation ability of a cyclist in real time, they define the state of fatigue of the cyclist as,

$$SOF = \frac{MVC - F_{max,iso}(t)}{MVC - F_{th,iso}} \tag{1.7}$$

where $F_{th,iso}$ is the equilibrium of Equation (1.6) at which the recovery and fatigue happen at an equal rate. This equilibrium is determined as,

$$F_{th,iso} = MVC\frac{R}{2k}(-1 + \sqrt{1 + 4\frac{k}{R}}) \tag{1.8}$$

The state of fatigue SOF, which is a number between 0 and 1, is considered as a state in the optimal control formulation. While the models presented in the paper mentioned above have basis in the literature, they are not validated using experiments. Moreover, in sports science community the notions of AWC and CP are more widely used.

In [16], the individual cyclist models presented are centered around AWC and CP. The dynamics of the remaining anaerobic energy of a cyclist is presented as,

$$a(t) = u - CP \tag{1.9}$$

where a is the remaining anaerobic energy and u is the cyclist's power. In this model recovery and fatigue happen at the same rate. However, in Section 1.1.3 it is mentioned that there are several studies suggesting that the recovery happens at a

slower rate than fatigue as mentioned in Section 1.1.3. Moreover, the authors in [16] assume the maximum power generation ability of a cyclist is constant. The results of a 3MT test rejects this assumption. If the power generation ability does not decay, then during the 3MT a cyclist is able to generate a constant level of power.

In the present study, using the concepts of Critical Power (CP) and Anaerobic Work Capacity (AWC), we propose an anaerobic energy recovery model that has a slower rate than fatigue and validate it using experimental data. Moreover, we propose a model for maximum power generation ability of a cyclist that is dependent on both the remaining anaerobic energy and the speed of a cyclist.

1.2 Contributions of this Dissertation

1. ***Developing practical mathematical models of fatigue and recovery in cycling***:

   In this dissertation, we investigate performance optimization for cyclists during time trial competitions, by formulating them as optimal control problems. To this end, a thorough literature review of the definitions, mechanisms, and models for fatigue and recovery is performed. The concepts of Anaerobic Work Capacity (AWC) and Critical Power (CP) are selected as the physiological parameters to be used in modeling a cyclist's fatigue and recovery during exercise. We then explain the design of a set of experimental protocols to determine how a cyclist expends and recovers anaerobic energy from the AWC. Out of 17 participants in the study, six subjects were able to successfully finish all the tests. Based on the experimental data, We propose a switching model for the dynamic of the remaining energy of a cyclist, in which recovery has a slower rate than fatigue. The rate of recovery depends on the cyclist's power level below

CP, which makes the model practical for real-time non-invasive performance assessment. Another important model derived from the experiments, is the maximum power generation ability of a cyclist. When a cyclist is fatigued, his or her maximum power generation ability is lower than a maximum effort when fully fresh. Additionally, there is an optimum pedaling cadence at which a cyclist's power generation ability is at its maximum. Pedaling below or above the optimum pedaling cadence, lowers one's ability to generate power. In this dissertation we propose a model for maximum power generation ability of a cyclist as a function of the remaining anaerobic energy and pedaling cadence, which is another contribution of this research.

2. ***Improving the travel time of a competitive amateur cyclist during an individual time trial by implementing an optimal controller***:

   We formulate an optimal control problem for a cyclist participating in an individual time trial competition using the generated dynamical models of fatigue and recovery from experimental data. The objective is to minimize time, constrained by both the bicycle and the cyclist's anaerobic energy dynamics. First, we derive the form of the optimal solution by adopting an analytical approach to the problem. Applying Pontryagin's Minimum Principle (PMP), we show that the optimal power for a cyclist can be either zero, CP, at maximum, or a power level that keeps the bicycle's velocity constant. We benefit from this result in the numerical simulation of the problem using Dynamic Programming, by limiting the solution space to the four modes found from the analytical solution. We then simulate a time trial competition using the model parameters for one of our subjects, who is a competitive amateur cyclist, and elevation profile from the 2019 National Duathlon Championship in Greenville SC. As a baseline, we

simulate the same elevation profile on a stationary bicycle trainer, and ask the same subject to ride over the simulated course in the laboratory environment with her own strategy. The optimal control simulated shows a 24% lower travel time compared to the baseline. However, in reality, a cyclist cannot perfectly follow the optimal power trajectory calculated by the controller. Therefore, in a first of its kind experiment, we set up a test environment in which the controller receives power, velocity, and position data from the cyclist, and sends back the optimal power to hold to the cyclist in real-time. In a pilot test the cyclist's travel time was reduced by 3% by following the controller's recommendation compared to the baseline test.

3. ***Showing that the mathematical optimal strategy during a team time trial race outperforms a popular empirical one***:

   A more complicated competition in cycling races is a Team Time Trial (TTT). In a team time trial, unlike the individual case, the cyclists in a team should cooperate with other. The important factor that affects the strategy of a team is the reduction in aerodynamic drag force acting on a cyclist who is trailing another team member with a close gap. The aerodynamic drag coefficient is a function of both the distance gap to a lead cyclist, and the position of a cyclist in the platoon. Using the previously calibrated models of fatigue and recovery, we first formulate an optimal control problem for a two-cyclist team. By applying the Direct Multiple Shooting method, we translate the optimal control problem to a Non-Linear Programming problem and solve it using the CasADi solver [71], and using the elevation profile of the 2019 National Duathlon Championship. The results show that while switching positions is necessary for the cyclists, the distance gap between them should be at the minimum safe gap. Then,

we expand the formulation to an n-cyclist team. In this case, distance gap between the cyclists is fixed, but the formation of them in the platoon is for the controller to decide. The respective optimal control problem is transformed to a Mixed-Integer Non-Linear Programming problem which is again solved with CasADi. For the purpose of comparison, we create a baseline solution where we apply a rule-based formation trajectory, and run the optimization problem with the team's acceleration as the only control input. This rule-based trajectory is based on the current popular strategy followed by cycling teams. This strategy directs the lead cyclist to frequently go to the back of the platoon after spending some time in the lead position [4]. Simulation results over the first 10 km of the 2019 National Duathlon Championship shows that the travel time of a three-cyclist team can be reduced by 2.3% compared to the baseline case. The optimal formation trajectory determined by the controller heavily depends on the elevation profile alongside the fatigue/recovery model parameters for each cyclist. Therefore, a rule-based strategy cannot be adopted for usage in every competition.

Chapter 2

Modeling and Experimental Design

A major part of this dissertation research focused on hypothesizing models for cyclists' fatigue and recovery, recruiting human subjects with proper Institutional Review Board (IRB) approvals, validating the hypothesis and calibrating the parameters of our chosen models using individualized data collected over many lab visits. This was a collaborative effort with another Ph.D. student. This chapter describes the test protocol and setup, models that were hypothesized, and their calibration process. In particular, we use the previously described three-minute-all-out test (3MT) to estimate the subjects' Critical Power (CP) and Anaerobic Work Capacity (AWC). The 3MT test also provides information regarding maximum power generation ability of a cyclist. We propose a model that relates the maximum power generation ability of a cyclist to his or her remaining anaerobic energy and pedaling speed. To determine the rate of recovery, we designed an interval test through which we can model the dependency of the recovery rate on a cyclist's power level, and recovery duration. These models help us assess the performance of a cyclist before, during, and after exercise, which is important in determining the optimal pacing strategy during a time trial effort.

2.1 Experimental Protocol

All of the experiments for this study were conducted in a laboratory setting on both Clemson and Furman University campuses. The tests were programmed on a RacerMate CompuTrainer [72] using Perfpro studio software application [73]. Subjects brought their own bicycles to be mounted on the CompuTrainer. The CompuTrainer applies resistance to the rear wheel, which can be programmed to follow any desired power profile. There are a few studies such as [74] that suggest the CompuTrainer's power measurement accuracy depends on a variety of parameters such as temperature and calibration procedure. Nevertheless, the CompuTrainer has been shown to be a valid device to estimate CP and AWC using the 3MT test in [75] and [76]. Figure 2.1 shows the experimental setup in our laboratory. The power and speed sensors are integrated in the CompuTrainer. Additionally, we used a Garmin heart rate [77], and a Moxy muscle oxygenation [41] sensor, shown in Figure 2.2, to collect data. These sensors were connected to the PerfPro software and measured heart rate and muscle oxygenation in real-time.

Figure 2.1: A view of the testing environment. The cyclist in this photo is not one of our subjects.

Figure 2.2: The Garmin heart rate (top), and Moxy muscle oxygenation (bottom) sensors used in the experiments.

The experimental protocol comprised of three tests namely, (i) a power ramp test to determine Gas Exchange Threshold (GET), (ii) a 3-minute all-out test (3MT) to determine CP and AWC, and (iii) an interval cycling test to determine the recovery of AWC. The ramp test involves incrementally (25 watts per minute) increasing the power at a constant cadence of 80 rpm until the subject is exhausted [15]. From the ramp test, oxygen uptake $\dot{V}_{O_2}$, defined as the volume of oxygen inhaled per minute per kilogram of body weight [34], alongside the volume of CO_2 exhaled per minute per kilogram of body ($\dot{V}_{CO_2}$), and the power are tracked. During the test, there is an abrupt increase in the ratio of volume of CO_2 exhaled to the volume of O_2 inhaled, which is the point at which blood lactate concentration starts to increase. This point is called the Gas Exchange Threshold (GET). The test is terminated when the subject pedals at least 5 rpm below the set cadence level of 80 rpm for 10 seconds (exhaustion). We then record the power at GET (P_{GET}) and the power at the end of the test (P_{max}). The average of these two powers (P_{cal}) was used to calibrate the 3MT test. The CompuTrainer's load was adjusted in a way that at 80 rpm, the subject's

power would be equal to P_{cal}. This method is adopted from [63] and [78].

In the next step, the subjects were tasked with performing the 3MT test. For each subject the CompuTrainer was calibrated using P_{cal}. Constant verbal encouragement was given to the subjects during the 3MT test to make sure they are exerting maximum power throughout the test. Each subject performed four 3MT tests. The first one served as a familiarization test for the subject to understand what the process is. Then, 3MT is performed three more time on three different days to make sure about the repeatability of the 3MT test. We then calculated CP from the average power of the last 30 seconds of the test, and AWC by integrating the power curve above CP.

The CP and AWC from the 3MT are then used to design the interval test for modeling the AWC recovery. The interval test was developed using the definitions of fatigue and recovery form Section 1.1.1 to derive mathematical models for recovery of AWC as well as the maximum power generation capacity of cyclists at any instant in a ride. The protocol was developed under the following assumptions:

- The 3MT test provides reliable estimates of CP and AWC.
- Exercise below CP utilizes the aerobic energy source, and results in recovery of AWC.
- The recovery of AWC below CP happens at a slower rate than its expenditure above CP.
- The *rate* of recovery depends on the recovery power and not the duration of recovery.
- The power held during recovery interval is averaged and assumed to be constant.

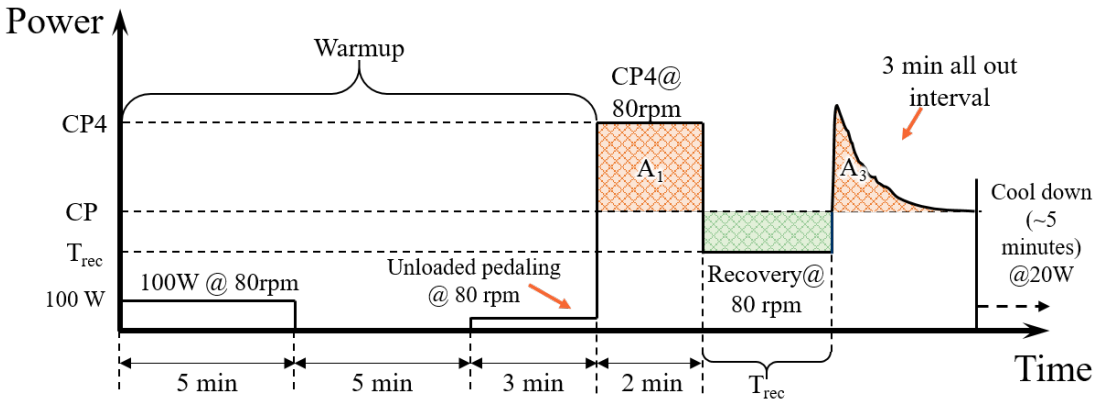

Figure 2.3: The power interval test protocol. After a warm-up period, the subject pedals at CP_4 for 2 minutes. Then the cyclist pedals at three different recovery power levels for different time intervals to recover energy. Following that, the subject performs a 3-min-all-out to burn all the remaining energy from AWC.

The interval tests were conducted at three different recovery powers (min power on Computrainer which was 80 Watts, 90% of power at GET (P_{GET}), and half way between P_{GET} and CP) and three durations (2 min, 6 min, 15 min). The power levels were adopted from [68] and recovery durations from [66]. There was at least 24 hours between two consecutive tests to ensure complete recovery. In the interval test protocol as shown in Figure 2.3, after a warm up of 10 minutes, there is a 2 minute interval at CP_4, the power at which all of the subject's AWC will be consumed in 4 minutes ($CP_4 = \frac{AWC}{240}$). The subject expends 50% of their AWC in the 2-min CP_4 interval and then recovers AWC at the mentioned recovery powers and durations. Following the recovery interval, the subject then performs a 3-min-all-out test to expend all of their remaining AWC. The amount of energy recovered in the recovery interval is then determined by subtracting AWC from the summation of areas above CP through the entire test.

On the first visit, the ramp test was conducted followed by a 3MT familiarization test. On the next three subsequent visits, a fresh 3MT was conducted from

which we can calculate the average CP and AWC. On the fifth visit, the interval test familiarization was conducted. On the nine subsequent visits, each subject performed the interval test protocol at three different recovery power levels and three time durations. We have conducted experiments on a total of 17 subjects. All of the subjects are cyclists who cycle at least 3 times a week, and are used to high intensity workout sessions. Each subject was scheduled for 14 one-hour-long visits to our laboratory. Because of the complexities of such scheduling, only 6 of the subjects were able to finish all of the tests. The test protocol was approved by Clemson University's Institutional Review Board (IRB) under protocol numbers IRB2016-169 and IRB2017-222. In order to be compliant with IRB policies we label our subjects by a number. The subjects who successfully finished all the experiments were Subs 6, 9, 11, 12, 14, 16.

2.2 Modeling Fatigue and Recovery

Let w be the amount of AWC remaining during exercise. The rate of change of w while expending energy above CP is given by the difference between the rider's power and CP. Recovery rate can be calculated similarly as assumed in [79]. However, it has been shown in [66] and [67] that recovery occurs at a slower rate than expenditure. For instance, if the cyclist is pedaling at a power level below the critical power, the amount of recovered energy will be less than the area between CP and the power curve. Thus, we propose to compute an adjusted recovery power using the amount of energy recovered given by,

$$P_{adj} \;=\; CP - \frac{w_{rec}}{T_{rec}} \tag{2.1}$$

where P_{adj} is the adjusted recovery power, and T_{rec} is the duration of recovery. Equation (2.1) can be rewritten to form an energy expenditure and recovery model as,

$$\frac{dw}{dt} = \begin{cases} -(P - CP) & P \geqslant CP \\ \\ -(P_{adj} - CP) & P < CP \end{cases} \tag{2.2}$$

where P is the power output of the cyclist.

Equation (2.2) represents a switching dynamic model of fatigue and recovery. To calculate the adjusted power we need a model that can provide P_{adj} at any power level in the recovery interval (i.e. below CP). The interval test was performed at three different power levels below CP, and three time durations to determine the effect of each on the rate of recovery. As mentioned before, one of the sensors used in the experiments was the Moxy oxygenation sensor. The sensor was placed on the thigh of each subject. This sensor measures SmO_2 which is the balance between oxygen delivery and consumption in muscle in percentage. SmO_2 is at its maximum when the cyclist is fresh, and decreases as the cyclist gets fatigued. In other words, a high SmO_2 demonstrates the cyclist's high amount of remaining energy from AWC. The data collector from this sensor shows that, at each recovery power level, SmO_2 rises to a certain level regardless of the time period of recovery as shown in Figure 2.4. In this figure, for each recovery power, the SmO_2 data series for all three recovery time durations are plotted together, from which we can observe a consistent steady state value for SmO_2. Therefore, the SmO_2 recovery, is dependent on the power level and not on recovery time. We extend this conclusion to the recovery dynamics of the anaerobic energy. Moreover, if it is assumed that w's rate of recovery depends on T_{rec}, the amount of recovered energy during recovery interval will depend on the recovery duration in the future which does not seem plausible. Therefore, we propose

that the recovery rate of w does not depend on the duration of the recovery interval T_{rec}.

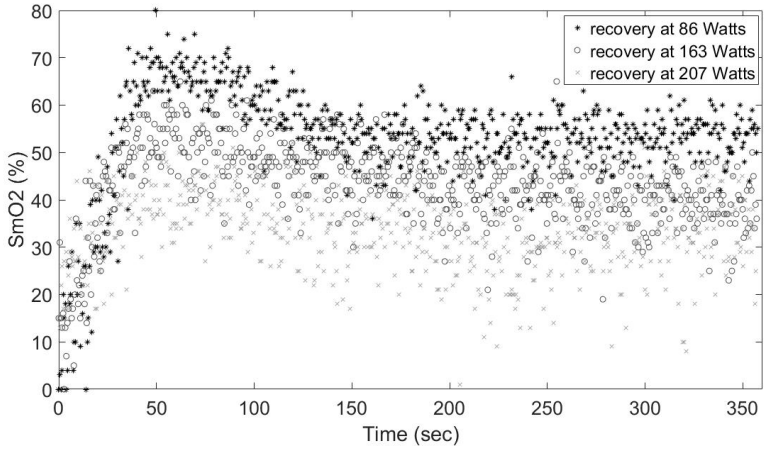

Figure 2.4: SmO_2 recovery during 6 min of recovery interval at three different power levels bellow sub 9's CP.

To arrive at a relationship between P_{adj} and the actual applied power by the rider, using Equation (2.1), P_{adj} can be calculated from the interval tests at each recovery power and plotted against the actual pedaling powers as in Figure 2.5. The following linear model provides a good fit to the experimental data from the interval tests,

$$P_{adj} \;=\; aP + b \tag{2.3}$$

where a and b are the model's constants. In order to find the recovery model parameters, the results of the interval tests are analyzed. As mentioned in before, it is assumed that the recovery model does not depend on time interval. Therefore, at each power level below CP, the adjusted power is calculated for the 3 time intervals and then averaged. By doing this we will have a plot of adjusted power versus actual applied power, consisting of 3 data points. Figure 2.5 represents the recovery model derived for Sub 14. Each of the three data points in this figure represents the average

adjusted power at each recovery power level for all three time intervals. The data point close to CP represents the adjusted power for the case where the subject pedals at halfway between P_{GET} and CP. Since the corresponding adjusted power is very close to CP we expect very little energy recovery at this level.

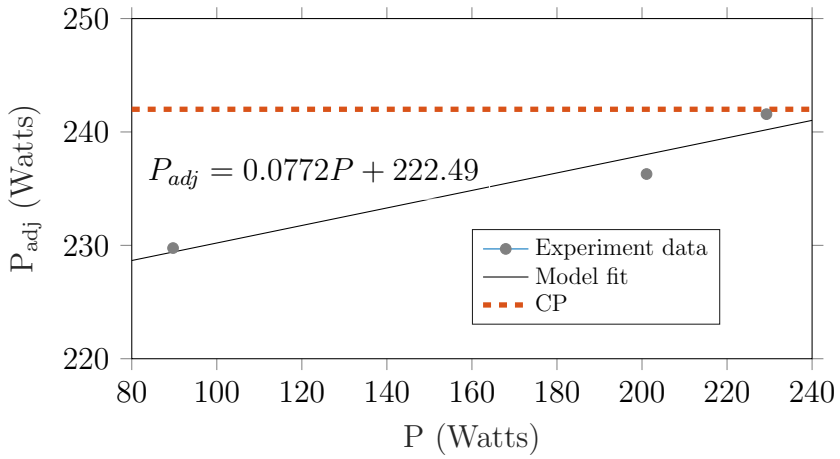

Figure 2.5: Recovery model plot for Sub 14.

2.3 Maximum Power Generation

Another parameter which is affected by the expenditure of AWC is the cyclist's ability to generate an instantaneous maximum power at any point during cycling. This is illustrated in the 3MT in Figure 1.2 where it is required for the subjects to pedal at their maximum power throughout the test. The power continuously decreases as a subject expends energy from AWC. Authors in [16] assumed a constant maximum power generation ability of 800 Watts regardless of the amount of energy remaining. If this assumption was to be valid, the 3MT profile would look completely different.

Using 3MT, a model of the maximum power vs. remaining energy w can be determined. The remaining energy at any instant during 3MT can be calculated

by computing the remaining area between the power plot and the CP line. The remaining energy w can then be plotted against power values in 3MT. Maximum power of the cyclist is applied 2 to 3 seconds into the test as it can be seen in Figure 1.2. Data points before the maximum power account for overcoming flywheel and aerobic inertia and are removed when fitting the model. The data is then fitted with a linear expression of the form,

$$P_{max}(t) \;=\; \alpha w(t) + CP \tag{2.4}$$

where w is the remaining energy of the cyclist's work capacity, and α is the model's constant. Figure 2.6 represents the relationship between maximum power generation ability and the remaining anaerobic energy of a cyclist.

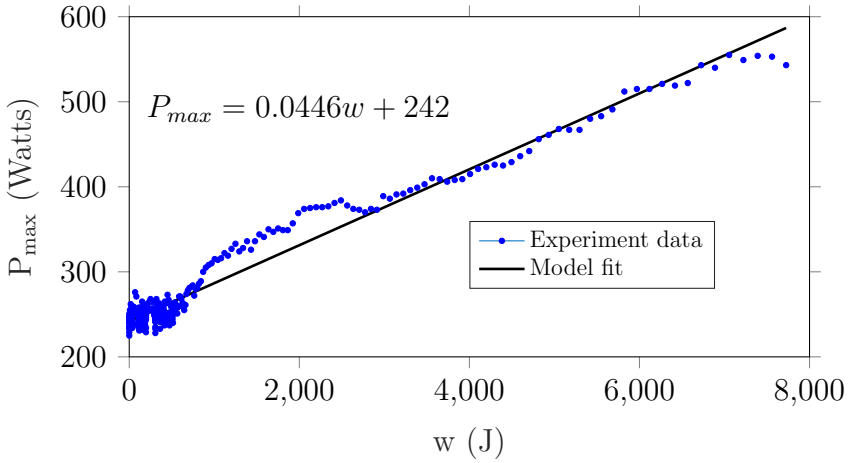

Figure 2.6: Power versus the remaining anaerobic energy of Sub 14 during the 3MT test.

There are several studies that suggest a relationship between maximum power, force and cadence in addition to the remaining anaerobic energy. In [2] authors present a survey of the literature on the maximal cyclist output (power, force, cadence). The standard experiment for deriving this relationship consists of a series of fresh sprint tests. Each sprint test is performed at a different braking force (CompuTrainer's

calibration force). To minimize the effect of fatigue, only the first few seconds of the test is taken into consideration. Figure 2.7 adapted from [2] demonstrates the test results for a subject performing fresh sprint tests at 4 different braking forces.

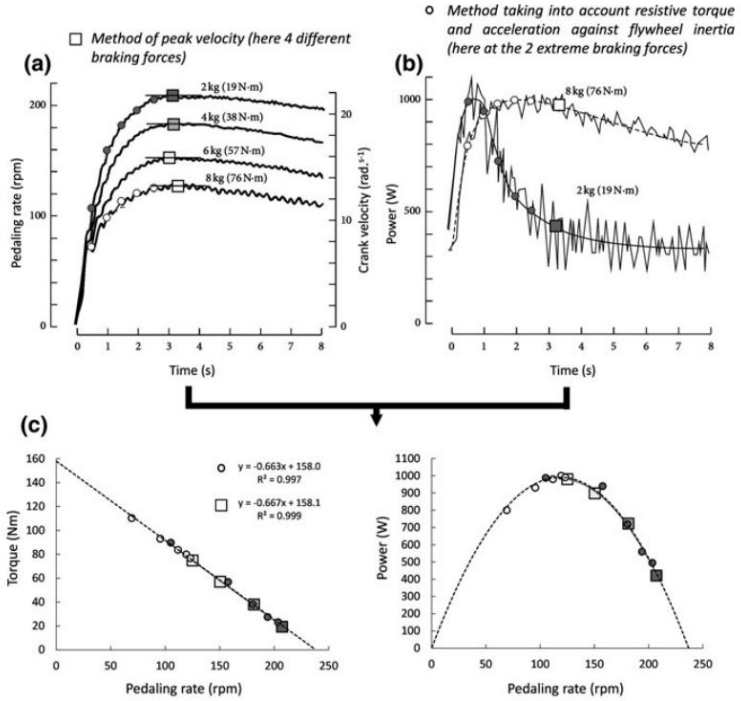

Figure 2.7: "a) Typical example of the time-course of the pedaling rate (or crank velocity) during a force-velocity test on a Monark cycle ergometer: 4 short sprints against 4 braking forces (in kg at the circumference of the flywheel and equivalent resistive torque in Nm at the crank axis). Squares correspond to the peak values and circles to the mean values on each complete cycle before. b) Time-power curves for the two extreme loads with the raw and filtered data (grey lines) and the same representation of the mean values on the five first complete crank cycles and at the peak velocities. c Mean value of torque, pedaling rate and power on these complete cycles (first 3 s of each sprint) can be used to plot torque- and power-velocity relationships. Note the good match in this example between the shape of these relationships for the two methods: one that considers only the peak velocity values of the 4 distinct sprints of panel a (squares: power corresponds to the product of peak velocity and braking force) and the other that considers all the cycles of the 2 sprints of panel b (circle: power measurement also takes into account the force to accelerate the flywheel inertia during the first phase of the sprint" [2]

It is observed from Figure 2.7(d) that if one plots the maximum power from each test against its corresponding cadence, a second degree polynomial relationship between them can be found as:

$$P = -(\frac{4P_{max}}{\omega_{max}^2})\omega^2 + (\frac{4P_{max}}{\omega_{max}}) \tag{2.5}$$

where (ω_{max}, P_{max}) denotes the extremum point of the polynomial. Subsequently, the

relationship between maximum force and cadence would be linear:

$$F = -(\frac{8P_{max}}{\omega_{max}^2})\omega + \frac{4P_{max}}{\omega_{max}} \tag{2.6}$$

Other studies also investigate the effect of fatigue of this parabolic relationship [80, 81, 82]. In [82] the authors show that if we repeat the short sprint test at different anaerobic energy levels and plot the parabolic function, the peak powers have a linear relationship with their respective remaining anaerobic energy. This is similar to our proposed model in Equation (2.4).

Similarly to power, maximum cadence also decreases with fatigue [80, 82]. As authors show in [82], maximal cadence is a linear function of the remaining anaerobic energy (w),

$$\omega_{max} = \alpha_\omega w + \omega_{max,f} \tag{2.7}$$

where α_ω is a model parameter and $\omega_{max,f}$ is the maximum cadence of the cyclist when AWC is fully depleted. Therefore, we propose the following model using Equations (2.4) and (2.7) as below,

$$P_{max} = -\left(\frac{4(\alpha w + CP)}{(\alpha_\omega w + \omega_{max,f})^2}\right)\omega^2 + \left(\frac{4(\alpha w + CP)}{(\alpha_\omega w + \omega_{max,f})^2}\right)\omega \tag{2.8}$$

It should be noted that we hypothesized Equation (2.8) after we collected our experimental data. Therefore, we made an assumption for us to be able to determine the constants α, α_C and $C_{max,f}$ post hoc. We assume the braking force applied by the CompuTrainer is set in a way that the subject is always at the peak power of the parabolic power-cadence function at each energy level in figure 2.8. Under this assumption we will be able to determine the model constants in Equation (2.8) with

a single 3MT. Figure 2.8 visualizes Equation (2.8) using Sub 14's model parameters which will later be used in our optimal control formulation as a constraint.

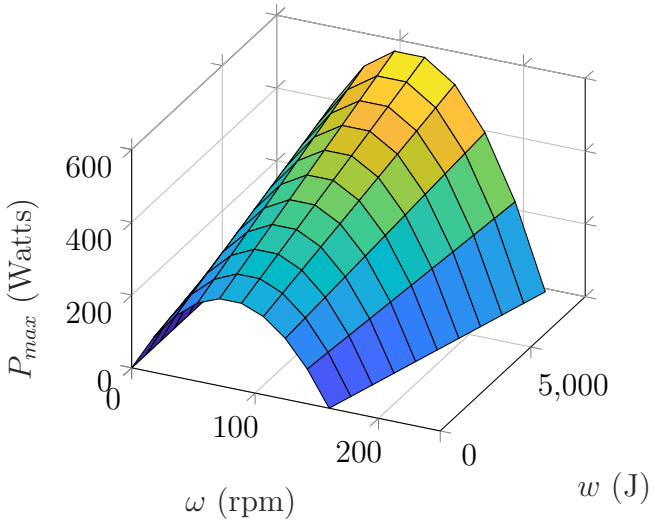

Figure 2.8: Maximum instantaneous power as a function of the cyclist's cadence and remaining anaerobic energy.

The summary of modeling results for all of the subjects is presented in Table 2.1. The reported values for CP, AWC, and constant parameters of the Equation (2.8) are the average of the three 3MT tests each subject performed.

Table 2.1: Experimentally determined parameters for the six subjects who successfully finished all of the 3-min-all-out and interval tests.

Subject	Sex	m (kg)	CP (Watts)	AWC (J)	a	b (Watts)	α (1/s)	$\alpha_\omega(rpm/J)$	$\omega_{max,f}(rpm)$
6	M	79	269	12030	0.11	237.5	0.037	0.017	139
9	M	63	233	10100	0.09	204.5	0.036	0.014	158
11	M	95	335	15092	0.08	300.9	0.039	0.01	163
12	M	70	217	5637	0.12	196.5	0.046	0.009	142
14	F	74	242	7841	0.08	222.5	0.044	0.008	164
16	M	51	206	9137	0.2	167.5	0.025	0.007	154

2.4 Conclusion

In this chapter, an experimental protocol was proposed to hypothesize and validate individualized mathematical models of fatigue and recovery. Six of the seventeen recruited human subjects were able to successfully finish all of the tests in the protocol. The protocol included 3MT and a recovery interval test which were repeated 3 and 9 times, respectively. Using the experimental data, a dynamic switching model for anaerobic energy expenditure and recovery was proposed that depends only on the power generated by a cyclist. Additionally, we presented a model to understand the maximum power generation ability of a cyclist that depends on two contributing factors. First, by expending energy from anaerobic sources, cyclists lose their ability to generate power. This is evident from the 3MT test where subjects were required to apply maximum power during the test, which declines throughout the test. Second, regardless of fatigue, the power generation ability of cyclists is constrained by pedaling cadence that is defined by a second-degree polynomial equation. This means that at very low and high cadence, a cyclist cannot generated much power. Integrating both of the contributing factors, we derived an equation to calculate maximum power generation ability of cyclists as a function of their remaining anaerobic energy and pedaling cadence.

The models proposed in this Chapter provide valuable information about the physical readiness of an athlete. Cyclists can track their individualized model parameters to better adjust their training routine. For instance, by measuring CP and AWC every month, cyclists can observe how their training is influencing these parameters. Then, in preparation for a race, they can design a specific training routine to improve these two parameters. In this dissertation, these models are used to formulate an optimal control problem for individual and team time trial competitions. As described

in the following chapters, having an estimate of a cyclist's remaining anaerobic energy and maximum power generation ability during a race, we can calculate the optimal power to hold, and send it back to the cyclist in real-time.

Chapter 3

Individual Time Trial

This Chapter presents an optimal control formulation and simulation for an individual Time Trial (TT) competition. Now that we have validated dynamic models of fatigue and recovery, the big question is what is the optimal strategy for a cyclist to finish a race in minimum time? When determining a rule-based strategy, one can think of pedaling at a constant power, or at a constant cadence as long as possible regardless of the elevation profile. On the other hand, when considering the elevation profile of the race, a cyclist may decide to pedal at a low power to "save" energy during the flat and downhill sections to have enough power for overcoming steep uphills. The question is how low should the recovery power be and for how long? To find the answer, we should have a mathematical approach to the questions. While our qualitative assessment of our performance and strategy can be helpful, in many cases it does not result in the best possible strategy.

Following an optimal controller's prescribed strategy can guarantee the best result. However, such controller is dependent on the accuracy of the physiological models of fatigue and recovery presented in the previous Chapter. While the models' representation of the fatigue and recovery process is acceptable, it is impossible to

model human muscle performance perfectly. That is because there are numerous factors affecting the process that might not be feasible to account for. Therefore, an optimal controller that is designed based on imperfect models may not provide the ultimate best solution. The main goal of this present Chapter is to find out whether a cyclist who follows the controller's recommendation can improve his or her performance in a TT compared to using a rule-based self strategy.

3.1 Optimal Control Formulation

In this section, we formulate the time trial race for a cyclist as an optimal control problem. The proposed system has three states: i) traveled distance s ii) velocity of the bicycle v and iii) remaining energy of the cyclist w, and a single input which is rider's power u,

$$\dot{x} = f\left(x(t), u(t)\right) = \begin{bmatrix} f_1 & f_2 & f_3 \end{bmatrix}^T \tag{3.1}$$

in which

$$x(t) = \begin{bmatrix} s(t) & v(t) & w(t) \end{bmatrix}^T \tag{3.2}$$

where $x(t)$ is the states vector. The function f is the nonlinear state-space model function, which relates the rate of change of the 3 states to the states and input. The first state function f_1 in Equation (3.1) is simply,

$$\frac{ds}{dt} = v \triangleq f_1 \tag{3.3}$$

Newton's second law can be used to write,

$$\frac{dv(t)}{dt} = \frac{u(t)}{mv(t)} - \frac{m_b}{m} g(\sin(\theta) + C_R \cos(\theta)) - \frac{1}{2m} C_d \rho A v(t)^2 \triangleq f_2 \tag{3.4}$$

where m_b is the mass of the bicycle and rider, m is the effective mass which is 1.4% greater than m_b, C_d is the aerodynamic drag coefficient, A is the frontal area, ρ is the density of air which is assumed to be constant and independent of the elevation, θ is the road slope which is positive for uphill and negative for downhill, and C_R is the coefficient of rolling resistance of the road.

Assuming 100% efficiency for the bicycle powertrain, we can equate $u(t)$ to the cyclist's power on the pedals. The advantage of using Equation (3.4) is that gear selection is not a factor in our formulation, which otherwise makes the optimization more complex. Note that the third state equation for time derivative of cyclist's remaining anaerobic energy is the previously represented by Equation (2.2),

$$f_3 \triangleq \frac{dw}{dt} = \begin{cases} -(u - CP) & u \geqslant CP \quad \text{(a)} \\ \\ -((au + b) - CP) & u < CP \quad \text{(b)} \end{cases} \tag{3.5}$$

Now we are able to formulate a minimum-time optimal control problem to formalize the pacing strategy in a time-trial. Therefore, the objective function to be minimized is time,

$$\min_{u(t)} \; J = \int_{t_0}^{t_f} dt \tag{3.6}$$

subject to,

$$\begin{array}{ll} \text{state-space model:} & \dot{x} = f(x(t), u(t)) \\ \text{velocity limits:} & 0 \leqslant v(t) \leqslant v_{max} \\ \text{remaining energy limits:} & 0 \leqslant w(t) \leqslant AWC \\ \text{rider's power limit:} & 0 \leqslant u(t) \leqslant u_{max}(w, \omega) \end{array} \tag{3.7}$$

where u_{max} is defined by Equation (2.8). In this formulation the final position is specified and fixed but the other two states v and w are left open at the final position. In the simulations, we assume the maximal speed v_{max} is constant during the trip, but our approach applies if v_{max} varies along the road for example during sharp corners.

3.2 Analytical Approach to the Optimal Control Problem

In this section we study the defined optimal control problem using the variational approach. According to Pontryagin's Minimum Principle (PMP), the necessary condition for the optimality of input u is that it minimizes the following Hamiltonian function,

$$H(x(t), u(t), \lambda(t)) = L(x(t), u(t)) + \lambda^T(t) \{f(x(t), u(t))\} \tag{3.8}$$

in which

$$\lambda = \begin{bmatrix} \lambda_1 & \lambda_2 & \lambda_3 \end{bmatrix}^T \tag{3.9}$$

where λ is the vector of co-state variables, L is the integrand in the cost function J in (3.6), and f is the vector on the right hand side of the state equations with components represented in Equations (3.3), (3.4), and (3.5). We also need to address the constraint of maximum power generation of the cyclist. The maximum power u_{max} is a function of state variable w and cadence ω as represented in (2.8). We need to translate ω to the state variable v for the constraint to be applicable in our formulation. Using the gear ratio of the bicycle in our experimental setup, we can write the bicycle's velocity v at each gear as,

$$v(t) = g_i R_{rear} \omega \tag{3.10}$$

where g_i is the gear ratio of the i^{th} gear, and R_{rear} is the rear wheel (tire thickness included) radius. The lab's bicycle has 21 gear combinations. We can combine Equations (3.10) and (2.8) to obtain the relationship between maximum power generation, remaining anaerobic energy, and the velocity as,

$$u_{max} = -\frac{4(\alpha w + CP)}{\left(\alpha_\omega w + \frac{v_{max}}{g_i R_{rear}}\right)^2}\left(\frac{v}{g_i R_{rear}}\right)^2 + \frac{4(\alpha w + CP)}{\left(\alpha_\omega w + \frac{v_{max}}{g_i R_{rear}}\right)^2}\frac{v}{g_i R_{rear}} \tag{3.11}$$

If we plot Equation (3.11) for each gear ratio, it will have a similar shape to Figure 2.8 except that cadence is translated to velocity. To make the formulation easier we want to build the constraint independent of the gear ratio, so we do not need to add the gear ratio as an additional control input. To this end, we take the

union of all 21 variations of Equation (3.11) given all 21 gear ratios. The reason behind performing this operation is shown in Figure 3.1. This 2D figure shows the parabolic relationship between power and velocity at a certain level of remaining anaerobic energy for two gear ratios. The operating point p1 is feasible when the 1st gear is selected, and not feasible when 2st gear is selected. The opposite is true for the second operating point p2. However, with proper gear changing strategy both operating points are reachable for the cyclist. Therefore, the union of the two parabolic functions for 1st and 2st gear is the feasible region.

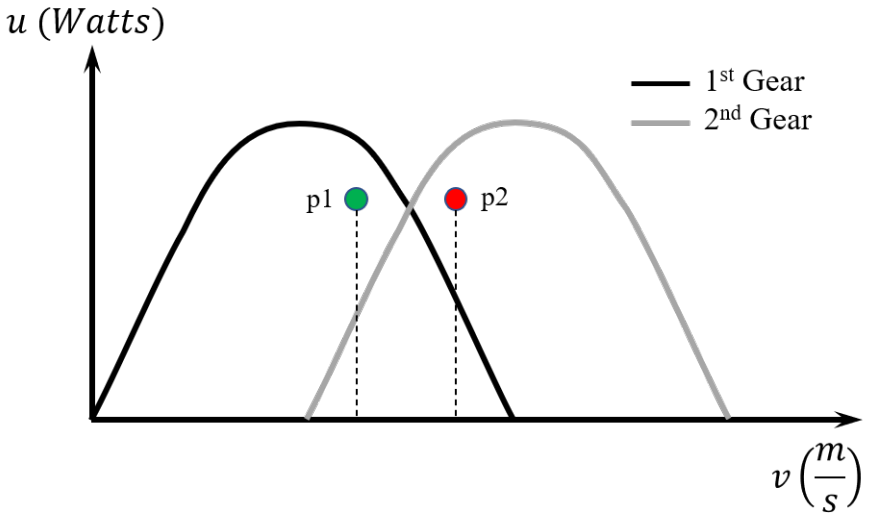

Figure 3.1: The power-velocity relationship at a given energy level for two gear ratios.

The result for taking the union of all 21 variations of Equation (3.11) with the parameters for Sub 14 is shown in Figure 3.2. Now, we have an inequality constraint as a function of the control u, the state v, and the state w variables. We can rewrite the constraint in a standard form as,

$$C(u, v, w) = u(t) - u_{max}(v(t), w(t)) \leqslant 0 \tag{3.12}$$

where $u_{max}(v, w)$ is defined by the surface in Figure 3.2. In the presence of such

an inequality constraint on control and state variables, the Hamiltonian needs to be augmented as follows [83],

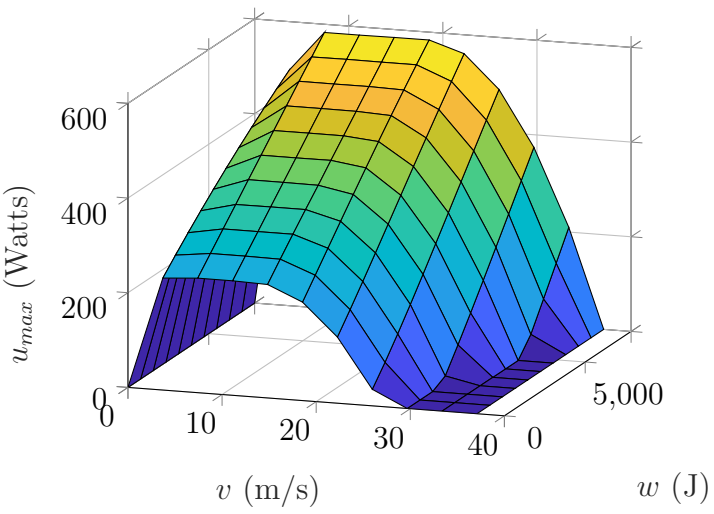

Figure 3.2: The constraint surface on the control input u as a function of the state variables v and w.

$$H = L + \lambda^T f + \mu C \tag{3.13}$$

where

$$\mu \begin{cases} \geqslant 0 & C = 0 \\ \\ = 0 & C < 0 \end{cases} \tag{3.14}$$

Additionally, the upper and lower limits on v and w presented in Equation

(3.7) should be taken into account as,

$$S(v,w) = \begin{bmatrix} v(t) - v_{max} \\ -v(t) \\ w(t) - AWC \\ -w(t) \end{bmatrix} \leqslant \vec{0} \tag{3.15}$$

Following [83], when constraints are not functions of the control input u, we take successive time derivatives of $S(v,w)$ and replace $\dot{v}$ and $\dot{w}$ with f_2 and f_3 ins Equations (3.4) and (3.5), respectively, until we obtain an expression that is explicitly dependent on u. In this case, the first derivative of $S(v,w)$ with respect to both v and w includes u. Then, we can treat $S^{(1)}(v,w)$ similarly to $C(v,w)$ and augment the Hamiltonian as,

$$H = L + \lambda^T f + \mu C + \eta^T S^{(1)} \tag{3.16}$$

where $\eta = \begin{bmatrix} \eta_1 & \eta_2 & \eta_3 & \eta_4 \end{bmatrix}^T$ must obey the following conditions,

$$\eta_i \begin{cases} \geqslant 0 \quad S_i^{(1)} = 0 \\ \qquad\qquad\qquad \text{for} \quad i = 1,2,3,4 \\ = 0 \quad S_i^{(1)} < 0 \end{cases} \tag{3.17}$$

It should be noted that the terms μC and $\eta^T S^{(1)}$ will always be zero in the Hamiltonian when constraints are met. The dynamics of the co-states follow,

$$\dot{\lambda}^T = -H_x \equiv -L_x - \lambda^T f_x - \mu C_x - \eta^T S_x^{(1)} \tag{3.18}$$

where the subscript x denotes the partial derivative with respect to the corresponding state variables. Rider's remaining energy model in Equation (3.5) switches between

fatigue and recovery conditions. Therefore, we have a switching Hamiltonian function between fatigue and recovery modes.

A necessary condition for optimality is that the control input u, minimizes the Hamiltonian. One can set the partial derivative of H with respect to u equal to zero. However, in this case because H is affine in u, the derivative with respect to u (H_u) does not depend on u.

$$H_u = \begin{cases} \frac{\lambda_2}{mv} - \lambda_3 + \frac{1}{mv}(\eta_1 - \eta_2) + (\eta_4 - \eta_3) + \mu & u \geqslant CP \\ \\ \frac{\lambda_2}{mv} - a\lambda_3 + \frac{1}{mv}(\eta_1 - \eta_2) + (\eta_4 - \eta_3) & u < CP \end{cases} \tag{3.19}$$

Note that the μ term only shows up when $u \geqslant CP$ because when $u < CP$ the constraint C is not active. Since Equation (3.19) does not depend on u, the optimal solution will be of the bang-singular-bang form; that is the Hamiltonian is minimized at extreme values of u with the exception of potential singular arcs in between.

When the Hamiltonian is affine in u, the sign of H_u indicates the optimal input value. As is shown in Equation (3.19), the sign of H_u depends on μ and η. When μ has a non-zero (positive) value, the constraint C in Equation (3.7) is active which means the optimal value for u is its maximum (u_{max}) regardless of the sign of the slope. When either η_1 or η_2 has a non-zero value, $S_1^{(1)}$ or $S_2^{(1)}$ is active. In that case, it can be shown that acceleration should be zero which means the optimal value for u is the power at which velocity is constant ($u_{\dot{v}=0}$). When either η_3 or η_4 has a non-zero value, $S_3^{(1)}$ or $S_4^{(1)}$ is active. In this case, it can be shown that $\dot{w}$ is zero which means the optimal input u will be at CP. The only cases left are when μ and η are all zero

and we can cross them off from Equation (3.19) and rewrite it as,

$$H_u = \begin{cases} \frac{\lambda_2}{mv} - \lambda_3 & u \geqslant CP \\ \\ \frac{\lambda_2}{mv} - a\lambda_3 & u < CP \end{cases} \tag{3.20}$$

The system of equations that should be solved are the state-space Equations (3.1) and (3.18), which provide 6 equations combined. The expanded version of the Equation (3.18) will be,

$$\begin{cases} \dot{\lambda_1} = g\lambda_2 g\frac{d\theta(s)}{ds}(\cos(\theta(s)) - C_R\sin(\theta(s))) \\ \\ \dot{\lambda_2} = -\lambda_1 + \frac{\lambda_2}{m_t}\left(\frac{u}{v^2} + C_d\rho A v\right) \\ \\ \dot{\lambda_3} = 0 \end{cases} \tag{3.21}$$

Now let's compare H_u in both fatigue and recovery modes. If H_u is positive, the minimum value of u minimizes the function. On the other hand, if H_u is negative, the maximum value of u minimizes the function. We can consider four cases,

Case I: $\frac{\lambda_2}{mv} - \lambda_3 < 0$ AND $\frac{\lambda_2}{mv} - a\lambda_3 < 0$

The slope in both fatigue and recovery modes are negative which means maximum value of u in each case minimizes the Hamiltonian. Now, we should see which one results in a lower value of Hamiltonian. In the fatigue mode the maximum input value is u_{max}, and in the recovery mode the maximum input value is CP,

$$H^* = \min\left\{H_{\text{fatigue}}(u_{max}), \quad H_{\text{recovery}}(CP)\right\} \tag{3.22}$$

where the subscripts of H differentiates between fatigue and recovery modes because the equations of the two modes are slightly different. If we substitute the aforementioned values of u we cannot decisively say which Hamiltonian is smaller. We can write the optimal input as,

$$u^* = \begin{cases} u_{max} & H_{\text{fatigue}}(u_{max}) < H_{\text{recovery}}(CP) \\ \\ CP & H_{\text{fatigue}}(u_{max}) > H_{\text{recovery}}(CP) \end{cases} \tag{3.23}$$

It should be noted that if the Hamiltonian is equal in both fatigue and recovery modes, we will have two optimal solutions.

Case II: $\frac{\lambda_2}{mv} - \lambda_3 > 0$ AND $\frac{\lambda_2}{mv} - a\lambda_3 > 0$

In this case, the input should take its minimum value in both cases, which will be CP and 0 for fatigue and recovery modes, respectively. The minimum Hamiltonian can be found from,

$$H^* = \min\{H_{\text{fatigue}}(CP), \quad H_{\text{recovery}}(0)\} \tag{3.24}$$

The optimal input value in this case will be:

$$u^* = \begin{cases} CP & H_{\text{fatigue}}(CP) < H_{\text{recovery}}(0) \\ \\ 0 & H_{\text{fatigue}}(CP) > H_{\text{recovery}}(0) \end{cases} \tag{3.25}$$

Similarly to the previous case, if the Hamiltonian is equal in both modes, we will have two optimal solutions.

Case III: $\frac{\lambda_2}{mv} - \lambda_3 > 0$ AND $\frac{\lambda_2}{mv} - a\lambda_3 < 0$

In this case, the input takes its minimum value in fatigue mode, and its maximum value in recovery mode. In both of these scenarios the input is CP, so we can decide,

$$u^* = CP \tag{3.26}$$

Case IV: $\frac{\lambda_2}{mv} - \lambda_3 < 0$ AND $\frac{\lambda_2}{mv} - a\lambda_3 > 0$

In this case, the input takes its maximum value in fatigue mode, and its minimum value in recovery mode, which will be u_{max} and 0, respectively. The minimum Hamiltonian can be found from,

$$H^* = \min\left\{H_{\text{fatigue}}(u_{max}), \quad H_{\text{recovery}}(0)\right\} \tag{3.27}$$

Th optimal input value in this case will be:

$$u^* = \begin{cases} u_{max} & H_{\text{fatigue}}(u_{max}) < H_{\text{recovery}}(0) \\ \\ 0 & H_{\text{fatigue}}(u_{max}) > H_{\text{recovery}}(0) \end{cases} \tag{3.28}$$

So far the optimal control input can take values of 0, CP, $u_{\dot{v}=0}$, and u_{max}. This means, when needed, the cyclist should recover at zero power. A hypothetical recovery scenario can be when the cyclist is on a steep downhill. However, there is still another case that is not investigated, which is a possible singularity condition.

Singular Arc: $\frac{\lambda_2}{mv} - \lambda_3 = 0$ OR $\frac{\lambda_2}{mv} - a\lambda_3 = 0$

Here we present the calculation for the case where the Hamiltonian's slope in the recovery or fatigue mode is zero. It can be shown that we get the exact same

final result for both modes. Therefore, we proceed with the recovery mode. During the possible singular condition in recovery mode we have,

$$\frac{\lambda_2}{mv} - a\lambda_3 = 0 \tag{3.29}$$

This equality needs to hold for an interval of time for a singular interval to exist. Therefore, its time derivative during that interval should also be zero. Setting the time derivative equal to zero and observing from Equation (3.21) that $\dot{\lambda}_3 = 0$ we get,

$$\frac{\dot{\lambda}_2}{v} - \frac{\lambda_2}{v^2}\dot{v} = 0 \tag{3.30}$$

We can substitute $\dot{\lambda}_2$ and $\dot{v}$ from Equations (3.21) and (3.4), respectively:

$$\begin{aligned} &\frac{1}{v}\Bigg[- \lambda_1 + \lambda_2 \frac{u}{mv^2} + \frac{\lambda_2}{m}(C_d\rho A)v \\ &- \frac{\lambda_2}{v}\left(\frac{u}{mv} - h(s) - \frac{1}{m}(C_d\rho A)v^2\right)\Bigg] = 0 \end{aligned} \tag{3.31}$$

Simplifying the equation above by using (3.29) yields,

$$\lambda_1 + am\lambda_3 h(s) + \frac{3}{2}(C_d\rho A)a\lambda_3 v^2 = 0 \tag{3.32}$$

Since input u does not appear in Equation (3.32), it becomes necessary to take the time-derivative again which yields,

$$\begin{aligned} &- \dot{\lambda}_1 + am\dot{\lambda}_3 h(s) + am\lambda_3 \frac{dh}{ds}v \\ &+ \frac{3}{2}a\dot{\lambda}_3(C_d\rho A)v^2 + 3a\lambda_3(C_d\rho A)v\dot{v} = 0 \end{aligned} \tag{3.33}$$

Simplifying by using Equation (3.21) yields,

$$3a\lambda_3(C_d\rho A)v\dot{v} = 0 \tag{3.34}$$

In Equation (3.34) only $\dot{v}$ can be zero. Therefore, during a potential singular interval the velocity must be a constant. The corresponding input power is obtained using Equation (3.4),

$$u^* = u_{\dot{v}=0} = mv\left(h(s) + \frac{1}{2m}(C_d\rho A)v^2\right) \tag{3.35}$$

which varies with the road grade.

Considering all of the cases discussed above, the optimal power can only take values from the vector below,

$$u^* = \begin{bmatrix} u_{max} \\ u_{\dot{v}=0} \\ CP \\ 0 \end{bmatrix} \tag{3.36}$$

Equation (3.36) provides the *necessary* conditions for optimality of u since it was based on a PMP analysis. It therefore suggests that the global minimizer at each time $u^*(t)$ must be one of these modes. This is an interesting insight and indicates that the optimal pedaling strategy may include one or more of the four modes of pedaling at maximal power, riding at CP, resting, or riding at a constant speed. While this insight is useful, it is difficult to analytically determine when the switching between these modes happens. Note that the three state equations in Equation (3.1) along with the three co-state equations in Equation (3.21) form a two point boundary value problem that is generally difficult to solve analytically. The switching dynamics of the

problem at hand creates additional challenges. Therefore, next we resort to numerical solution of the optimal control problem via dynamic programming. The above PMP analysis proves valuable in limiting the input space in DP process to only the modes described by Equation (3.36) which significantly reduces the computational burden of DP.

3.3 Numerical Solution of the Problem

In our DP implementation, at every step in distance, the state variables are quantized between their minimum and maximum. On the other hand, the control variable u is only quantized at the four power levels in Equation (3.36) without the loss of optimality, which will significantly reduce the required memory and time of the computing process. First, the state space model in Equation (3.1) is discretized. Since the final destination is known, we pick distance as the independent variable and discretize it at regular intervals $\Delta s = 10$ m. With a zero-order hold on input in between sampling intervals we obtain the following discretized state-space equations:

$$t_{i+1} = t_i + \frac{\Delta s}{v_i} \tag{3.37}$$

$$v_{i+1} \;=\; v_i + \frac{\Delta s}{v_i}\left(\frac{u_i}{m_t v_i} - g(sin(\theta_i) + \mu cos(\theta_i)) - \frac{0.5 C_d \rho A}{m_t} v_i^2\right) \tag{3.38}$$

$$\begin{cases} w_{i+1} = w_i - \frac{\Delta s}{v_i}(u_i - CP) & u_i \geqslant CP \\ \\ w_{i+1} = w_i - \frac{\Delta s}{v_i}(a u_i + b - CP) & u_i < CP \end{cases} \tag{3.39}$$

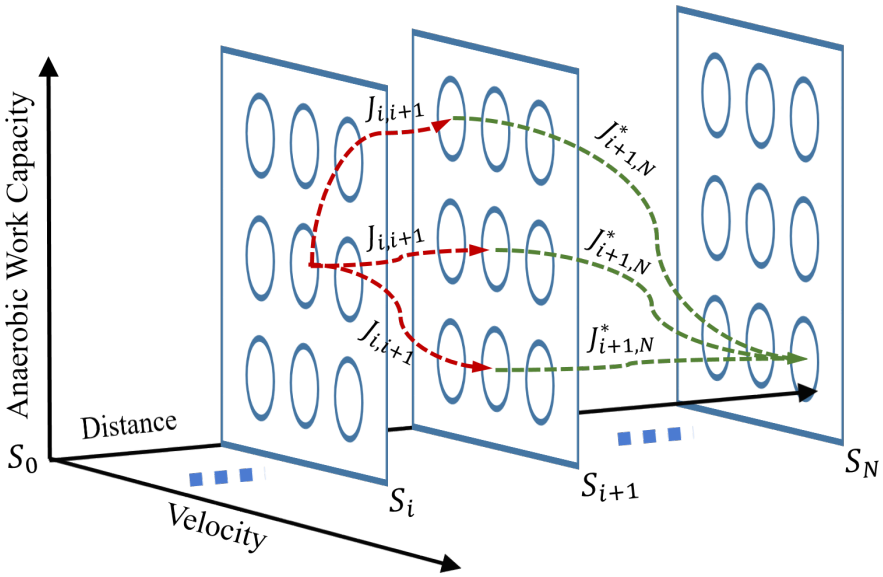

Figure 3.3: Demonstration of use of Bellman's principle of optimality in dynamic programming.

The cost function in Equation (3.6) is rewritten with position as the independent variable and discretized as follows[1],

$$J_N = \sum_{i=0}^{i=N} \frac{\Delta s_i}{v_i} \tag{3.40}$$

According to the Bellman's principle of optimality [84], when a system is on its optimal path from an initial state to a final state, regardless of any past decision or state, it should follow an optimal policy for the remainder of the route. Therefore, in dynamic programming, to find the optimal state trajectory, one can begin from the final state and move backward and calculate the optimal cost-to-go from any state to the final step. Figure 3.3 demonstrates the backward dynamic programming method based on the Bellman's principle of optimality. The optimal costs from all of the

[1]When implementing this objective function in DP, we sometimes observed chattering in the power trajectory. This chattering can be the optimal solution or due to the coarse quantization of control input to only four (optimal) modes. To achieve a practical power trajectory for a cyclist, we added a regularization term to the cost that penalizes the change in control input from stage to stage multiplied by a small penalty weight. The weight was carefully tuned to minimize the impact of the regularization term on the value of the objective function.

nodes at s_{i+1} to the final state at s_N are stored as $J^*_{i+1,N}$. Then, cost-to-go from every node at s_i to all of the nodes at s_{i+1} is calculated and the optimal value among them is stored at the specified node at s_i. This process is repeated backwards to the beginning of the route. Subsequently, in a forward DP sweep, the optimal action at each discretized state node will be known. Let's denote the optimal cost-to-go from specific velocity and energy states at step s_{i+1} to s_N by $J^*_{i+1,N}$. Then, the optimal trajectory from step s_i to s_N will be,

$$J^*_{i,N} = \min_{u_i} \ [J_{i,i+1} + J^*_{i+1,N}(x)] \tag{3.41}$$

where

$$J^*_{i+1,N} = \min_{u_{i+1},u_{i+2},\ldots,u_{N-1}} \ [J_{i+1,N}] \tag{3.42}$$

The DP formulation was then coded in MATLAB. At every step in distance, velocity v is quantized to 300 nodes spaced uniformly in the interval [1, 20] m/s. The choice of minimum velocity at $1m/s$ is because i) speeds closer to zero cause numerical issues as v appears in the denominator in the discretized equations of motion ii) during a time-trial the athlete is unlikely to pedal at lower speeds. Anaerobic energy w is quantized into 600 nodes spread uniformly between 0 and the Sub 14th AWC ($7841J$). As discussed earlier, the input power u is also quantized to 4 values the the levels indicated by Equation (3.36).

When at the distance s_i from the initial position, v_i and w_i states move to v_{i+1} and w_{i+1} by applying an input u_i. The resultant states at step s_{i+1} will not necessarily attain the quantized values of states v and w. Therefore, we implemented a stochastic transition to the neighboring nodes on the $v - w$ plane. The transition method is adopted from [3] and is shown in Figure 3.4. In this figure, the red circle shows

the resultant state which is not on a quantized value of states v and w. According to [3], the transition cost is calculated as a weighted summation of the costs at the neighboring nodes as,

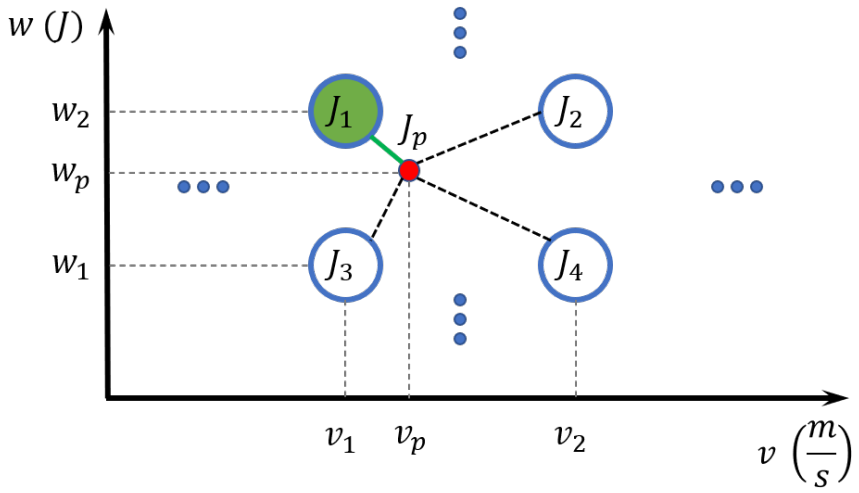

Figure 3.4: The schematic of the stochastic transition method presented in [3] using the neighboring nodes.

$$
\begin{aligned}
J_p = &\left(\frac{v_p - v_1}{v_2 - v_1}\right)\left(1 - \frac{w_p - w_1}{w_2 - w_1}\right) J_1 + \\
&\left(\frac{v_p - v_1}{v_2 - v_1}\right)\left(\frac{w_p - w_1}{w_2 - w_1}\right) J_2 + \\
&\left(1 - \frac{v_p - v_1}{v_2 - v_1}\right)\left(1 - \frac{w_p - w_1}{w_2 - w_1}\right) J_3 + \\
&\left(\frac{v_p - v_1}{v_2 - v_1}\right)\left(\frac{w_p - w_1}{w_2 - w_1}\right) J_4
\end{aligned}
\tag{3.43}
$$

The calculated cost J_p is then stored in the nearest neighbor [3], which in Figure 3.4. is node 1 specified by green color.

Initially, the cyclist starts from the minimum velocity, and his/her remaining energy is initialized at AWC. The DP simulation was ran on a desktop computer with a 3.2GHz Intel core i5 CPU, and 12GB of RAM. The computation time for our

longest cycling route (18km) was 53 min and 45 sec. This is thanks to the PMP results that allowed us to significantly reduce the input quantization. Without it the computation time would be close to two days.

3.4 Results and Discussion

3.4.1 Simulating Optimal Pacing

To illustrate the nature of optimal solution, we first found the optimal pace over 4 km roads with three basic elevation profiles: a flat road, a road with a 5% grade climb, and a road with two hills. Figure 3.5 shows the three scenarios and the results based on Sub 14 data. Optimal power u, remaining anaerobic energy w, and velocity v are shown in each case. The figure also shows which one of the four optimal control mode was chosen in the u_{mode} subplot, in which which values of 1, 2, 3, and 4 correspond respectively to the control u equaling, 0, CP, $u_{\dot{v}=0}$, and u_{max}.

On the flat road, the optimal strategy is to go all-out till all anaerobic reserves are depleted and then continue with critical power. In this case, the maximum power constraint is activated and the power trajectory stays on the constraint. More interestingly, during the ramp course, the optimal pacing strategy benefits from elevation preview. The cyclist burns only 2% of anaerobic energy in the starting line to get to the velocity that can be then maintained by applying CP. The reserved energy comes to use during the ascent over the hill, by the end of which all of the AWC is expended and the cyclist pedals at CP towards the end. During the simulation over a course with two uphill sections, having known about the upcoming downhill, the controller recommends the cyclist to burn most of the anaerobic energy. Then during the downhill, the subject recovers 8% of the AWC to overcome the second hill. In

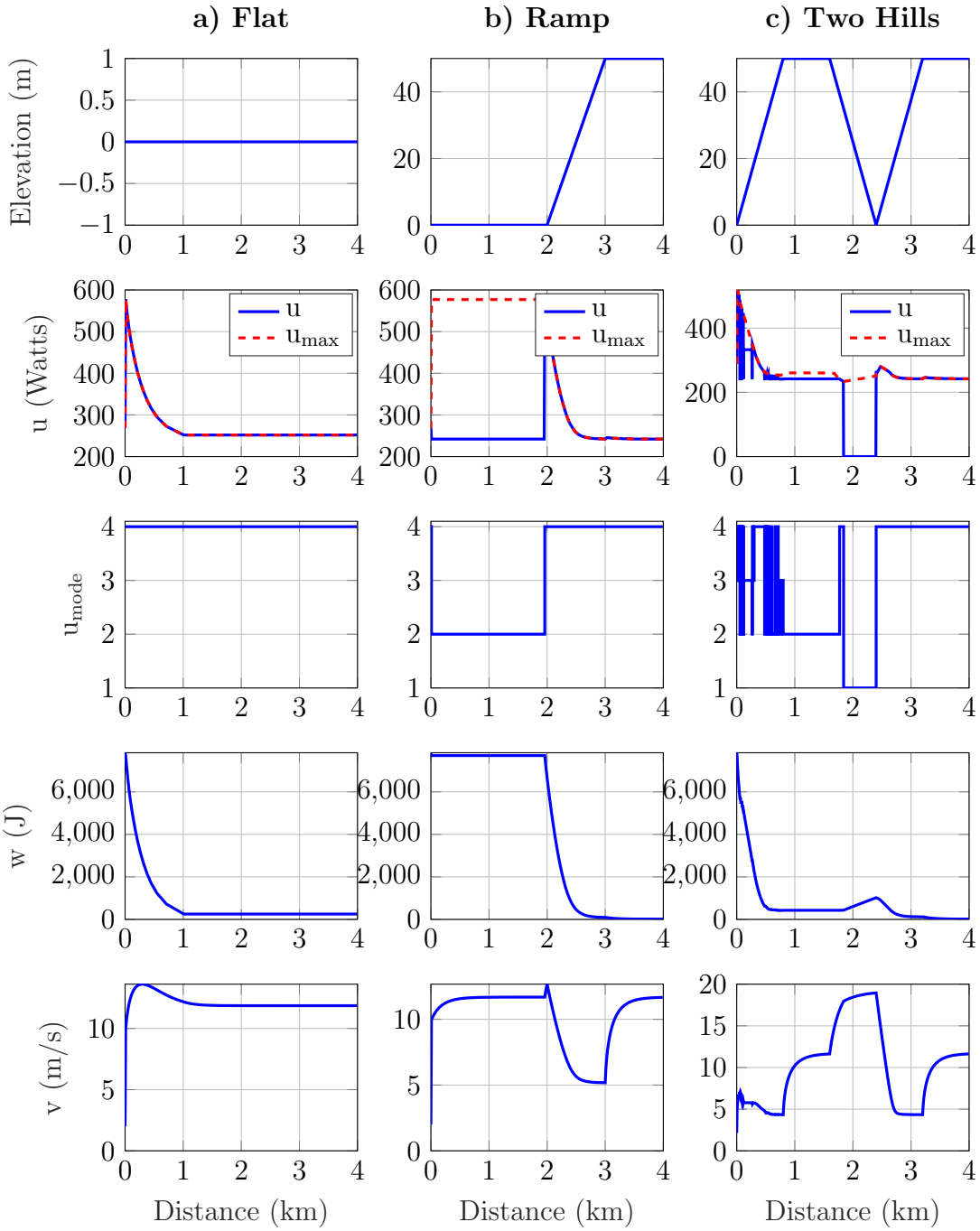

Figure 3.5: DP simulation results over three elevation profiles. Sub14 model was used in this set of simulations.

this case, all four modes of optimal power are applied.

3.4.2 Baseline Performance Captured by an Experiment

We had the opportunity to simulate the cycling course of the 2019 Duathlon National Championship in Greenville, South Carolina on our CompuTrainer. The elevation profile of this course is presented in Figure 3.6. We ran this experiment with Sub 14 by requesting the subject to ride with her own strategy as the baseline test[2]. During the test, she was receiving velocity, distance, power, elevation, and heart rate data in real-time via the interface depicted in Figure 2.1.

The subject managed to finish the course in *34 min 8 sec*. However, our DP simulation suggests that if she followed the optimal power provided by the DP, she would have finished the course in *25 min 56 sec*. An important observation from this test is that the subject's self strategy lacks consistency in applying power. During the first 5 km of the course in the self-paced scenario, the average power of the cyclists is 230 Watts, whereas during the last 5 km it is 190 Watts. Both of these values are below the Subject's critical power (242 Watts). However, the optimal simulation suggests that except for several short periods of maximal effort and recovery, power should remain at CP. While velocity profile in the simulation is always higher than the subject's velocity, both profiles have a similar trend during the course which is dictated by the elevation profile. The difference between the velocity profiles can be explained by the the short frequent maximal efforts that increases the cyclist's velocity. The average power of the optimal strategy is 240 Watts which is only 28

[2]One of the shortcomings of utilizing Computrainer is that it does not model drag force during a ride. Therefore, the drag term in Equation (3.38) should be removed. Also, when the subject is riding downhill, the CompuTrainer cannot accelerate the bicycle as would happen on a real road. Therefore, besides removing the negative resistance force due to downhill section of the course, the calibrated resistance force of 15.5 N is added to Equation (3.38) instead of the drag force. This force is imposed constantly by the CompuTrainer and is set during the calibration process.

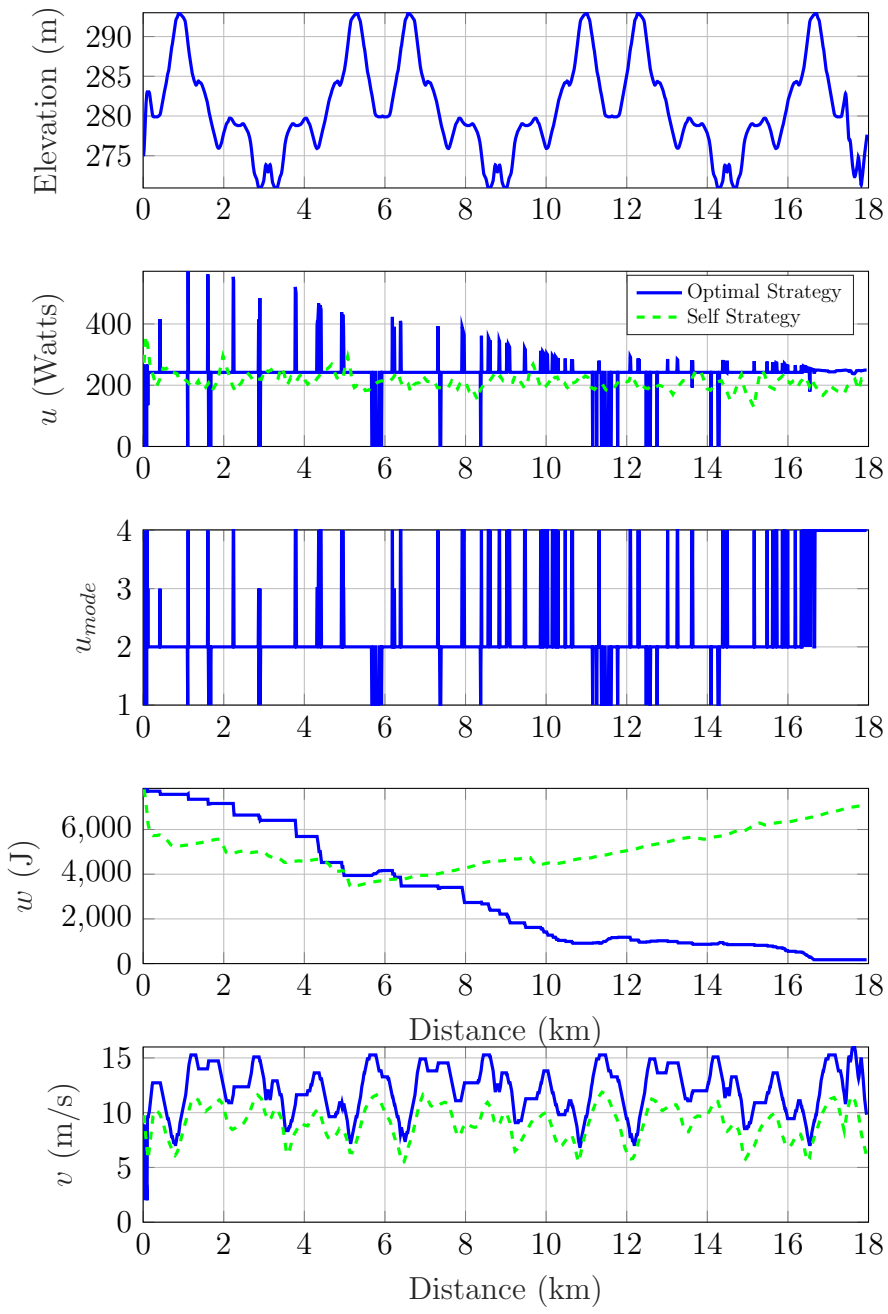

Figure 3.6: Power and energy trajectory differences between sub 14's self strategy and the optimal simulation on the Greenville Duathlon course.

Watts greater than the total average of the self strategy case.

Also, because the cyclist was pedaling below CP for most parts of the course, she recovered almost all of her anaerobic energy at the end which is the against the optimal strategy. Although our subject was familiar with the route and cycles around four times a week, she is not a professional athlete and lacks high level training, which could be one reason for her lack of pace in spending anaerobic energy. Nevertheless, pacing over long hilly courses can be a challenge for professional athletes, and our proposed optimal strategy could be used for coaching or even real-time guidance of cyclists.

3.4.3 Controller Implementation

In addition to simulation we prepared the test setup to implement the controller in real-time use. The benefit of using DP is that once we calculate the backward solution, we can store it as a lookup table. This lookup table can be used at any point in time during a race. If we have measurements of a cyclist's power, velocity, and position, we can estimate the remaining anaerobic energy at that time. Then, we can refer to the backward solution of DP and find out what the optimal power to hold should be at that position. In order to implement this real-time controller, we first needed access to the power, velocity, and position data from the CompuTrainer's software. The challenge was that PerfPro software was not capable of logging data into a file during the exercise. It only saved the exercise data on an Excel file after the work out is finished. However, PerfPro visualizes the real-time data on its graphical user interface as shown in Figure 3.7. Therefore, we set up a software that took a screen shot of PerPro's user interface every 0.5 seconds. Then, an image processing code was run in MATLAB to collect power, velocity, and position data from each

picture.

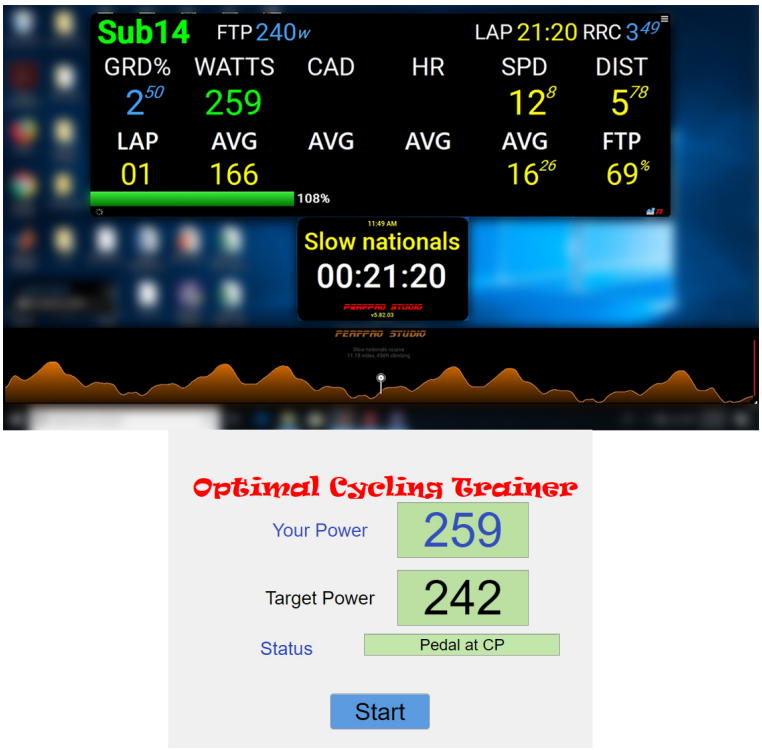

Figure 3.7: The PerfPro user interface on top, and the MATLAB interface designed to communicate information with the cyclist in the bottom.

The position interval of DP was set at 100 m. During each interval, we calculated the average power and velocity of the cyclist, and estimated the remaining anaerobic energy. With that information, optimal power to hold for the next position interval was calculated from the stored lookup table. This power level was sent to the cyclist to follow. We designed a MATLAB graphical interface to communicate information to the cyclist. The interface showed optimal power to hold, applied power by the cyclist, and written status of the optimal power suggestion.

We had a chance to perform a pilot test with Sub 14 by suggesting optimal power to hold in real-time. Similarly to the baseline test presented in Section 3.4.2, we simulated the elevation profile of the 2019 National Duathlon Championship on the CompuTrainer. The difference was that this time the cyclists was instructed

to only look at the MATLAB user interface and follow the optimal power. This is because if the subject knew her position in the course, she might have included her own strategy in the process. In that pilot test, Sub 14's travel time was reduced by 3% when following the optimal power suggestion. However, after the test, we found out that there was a minor error in the stored backward solution of DP. That is why the results of that test is not presented in this dissertation.

This implementation was the first known attempt of its kind on pacing a cyclist during a time trial by providing real-time optimal power suggestions. In the future of this study, the controller implementation test can be done with multiple subjects to verify the effectiveness of the proposed optimal controller.

3.5 Conclusion

In this chapter, the previously validated models of fatigue and recovery from Chapter 2 were used to formulate an individual time trial (TT) race as an optimal control problem with three states (position, velocity, and remaining anaerobic energy), and a single input (a cyclist's power). Initially, the problem was approached analytically using the Pontryagin's Minimum Principle (PMP). By applying PMP, we showed that there are only four optimal modes for a cyclist's power during a TT race. Power can be zero, at CP, at a power level that keeps the velocity constant, or at maximum power generation ability. There are two takeaways from this analytical solution. First, it helps cyclists develop a rule-based strategy knowing that they should not exert any power level other than the four modes presented. Second, in the numerical simulation of the problem, we can limit the solution set to these four power values and reduce the computation time significantly. Dynamic Programming (DP) was used for the numerical simulation of the problem. We selected the ele-

vation profile of the 2019 National Duathlon Championship in Greenville, SC which was simulated on a CompuTrainer. Results from simulating over this elevation profile using one of our human subjects' individual model shows 24% improvement in travel time compared to a baseline test, where the same subject was instructed to ride over the simulated course with her own strategy.

In order to realistically assess its benefits, the optimal pacer was implemented during an experiment, where optimal power to hold was given to the subject in real-time during the race over the simulated course on the CompuTrainer. The results of a pilot test showed a 3% reduction in the subject's travel time compared to the baseline test, which was promising. In the future, more tests with several subjects are needed to validate the effectiveness of the optimal pacer.

Chapter 4

Team Time Trial

A Team Time Trial (TTT) is a road cycling competition in which a team of 2 to 10 cyclists run against the clock as described by Union Cycliste Internationale (UCI). The fundamental difference between a Team Time Trial and an Individual Time Trial is that the team members in TTT benefit from drafting behind each other. This means riding in close distances between each other which reduces the aerodynamic drag force on the trailing cyclists. The reduction in the aerodynamic drag in drafting depends on two factors: 1) the distance to the preceding cyclist, and 2) the position of the cyclist in the platoon. Several studies have investigated the effects of these factors on the drag coefficient [4, 85, 86].

Therefore, it is crucial for cycling teams to strategize switching their position in the platoon. For instance, a simple periodic strategy would be for a cyclist in the leading position to go to the back of the platoon, which is repeated by every cyclist in the team. Understanding the strength of the team members is a key to finding the best strategy. Should the strongest cyclist mostly be in the leading position, or not? How long each formation should be maintained? The fatigue and recovery models presented in this dissertation can be very useful to strategize a TTT. Our

proposed approach involves an optimal controller that has access to power, velocity, and position data from the athletes, and estimates their remaining anaerobic energy, and determines the optimal formation for the team at every time step. In this chapter, we present an optimal control formulation that can be generalized for an n-cyclist team. The first step is to establish the cyclist and aerodynamic drag models.

4.1 Modeling

4.1.1 Individual Cyclist Models

The same individual models of fatigue and recovery that were presented in Chapter 3 are used for the problem of Team Time Trial. For completeness, we will review this model again here. The rate of energy expenditure above CP is the difference between the cyclist's power and CP. However, recovery happens at a slower rate than fatigue, which is accounted for in our model by adjusted powers below CP,

$$\frac{dw}{dt} = \begin{cases} -(p - CP) & p \geqslant CP \\ \\ -((ap + b) - CP) & p < CP \end{cases} \tag{4.1}$$

where w is the remaining anaerobic energy, and p is the cyclist's power. The parameters a and b are the model constants to be determined individually for each cyclist using experimental data. Combining fatigue and recovery models, we can define an adjusted power function as below,

$$\mathcal{P} = \begin{cases} p & p \geqslant CP \\ \\ ap + b & p < CP \end{cases} \tag{4.2}$$

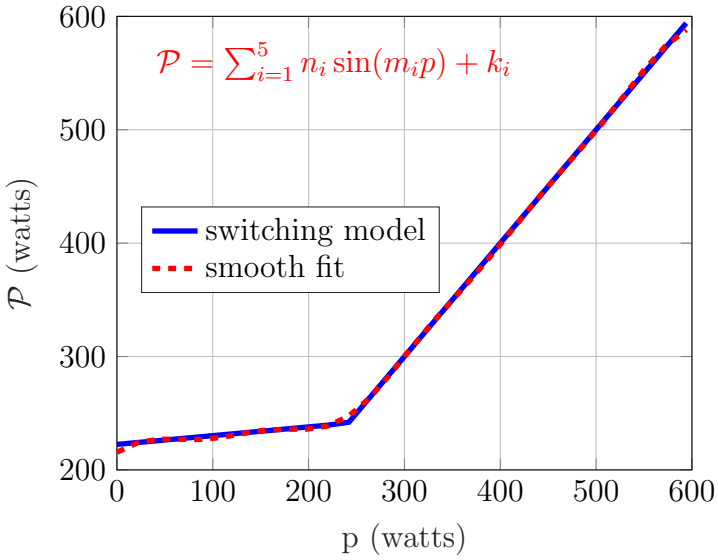

Figure 4.1: The switching function $\mathcal{P}$ for fatigue and recovery with the smooth fit.

Equation (4.1) can be rewritten as,

$$\dot{w} = \mathcal{P}(p) - CP \tag{4.3}$$

The switching function $\mathcal{P}$ is shown in Figure 4.1 as a function of a cyclist's power p. Since $\mathcal{P}$ has a non-differentiable point at CP, a smooth function of the sum of five sinusoidal terms is fitted to the data in Figure 4.1 to ensure differentiability during numerical optimization.

An important aspect of modeling a cyclist's physical ability is the maximum power generation capability which is diminished by expending energy from AWC. We employ the same maximum power generation constraint presented in Chapter 3 that depends on the amount of the remaining anaerobic energy as well as bicycle's speed as shown in Figure 3.2.

4.1.2 Aerodynamic Drag Coefficient During Drafting

The central part of our approach models how the aerodynamic drag forces change with respect to the distance gap between cyclists and their position in the platoon. The aerodynamic drag force is calculated as,

$$f_{drag} = 0.5\rho C_D A v^2 \tag{4.4}$$

where ρ is the air density, C_D is the aerodynamic drag coefficient, A is the frontal area of the bicycle while the cyclist is seating on it, and v is the cyclist's velocity. Assuming the cyclist remains in an optimal posture to expose the least possible frontal area to the air stream, the only action that minimizes drag, is a reduction in the drag coefficient by riding behind another cyclist in the team.

There are three ways to estimate the aerodynamic drag coefficient imposed on each cyclist in a team including field tests, wind tunnel tests, and Computational Fluid Dynamics (CFD) methods [4]. In the present study we adopt the wind tunnel test results for cyclists in a straight line from [4]. Figure 4.2 shows the drag coefficient for the cyclists in a two-cyclist platoon with respect to the changes in the distance gap. In addition to the distance, drag coefficient depends on the position of a cyclist in the platoon. If we fix the distance gap between the cyclists in a platoon, the drag coefficient imposed on each is very different at various positions in the platoon. Figure 4.3 shows the drag coefficient at each position in a 6-cyclist platoon given a distance gap of 50 cm between the cyclists [4].

Formulating an optimal control problem that in addition to velocity and energy of each cyclists, includes the distance gap between them as state variables can be very complex. Determining the order of cyclists in the platoon with respect to their distance gap with each other is another source of complexity that increases the

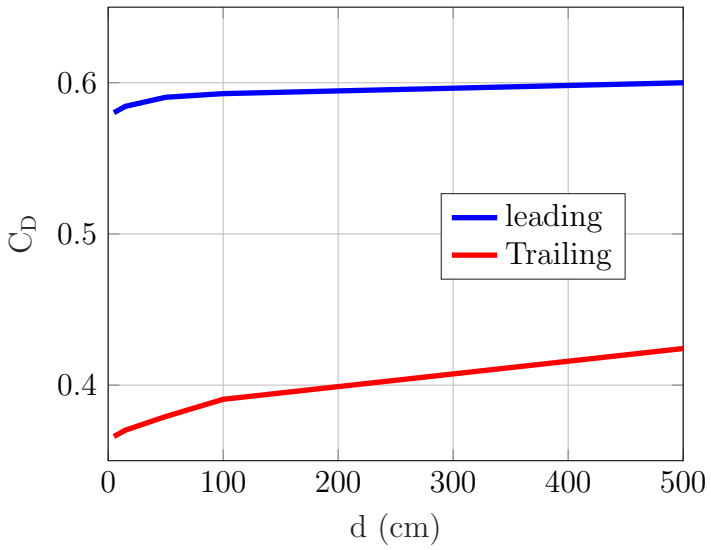

Figure 4.2: The drag coefficient for the leading and the trailing cyclists in a two-cyclist team as a function of the distance gap between the cyclists [4].

decision variables dramatically. Even after resolving all the mentioned challenges, it will be computationally costly to simulate a system with a high number of optimization variables. Therefore, we first study a less challenging case study of a two-cyclist team, where we hope to achieve useful insights that can help us develop an applicable generalized system of equations for an n-cyclist team.

4.2 Two-Cyclist Team

4.2.1 Problem Formulation

Consider two cyclists in a straight line. In a take over maneuver, a cyclist needs to change lanes which will require including the lateral dynamics of the bicycle in addition to longitudinal. This will add additional states to the state-space and therefore adds complexity to the optimal control formulation. In this study, we propose a formulation that only requires longitudinal dynamics by handing over the

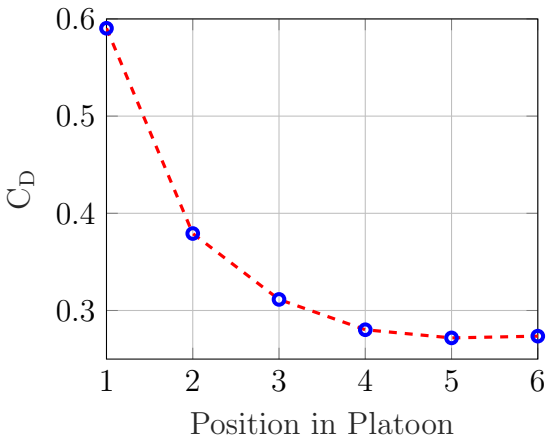

Figure 4.3: The drag coefficient as a function of the position of a cyclist in a 6-cyclist platoon with cyclists having a 50cm distance gap between each other [4].

steering responsibility to the cyclist.

For the case of a two-cyclist team, the proposed system has 6 states,

$$x = \begin{bmatrix} s_1 & v_1 & w_1 & d & v_2 & w_2 \end{bmatrix}^T \tag{4.5}$$

where s, v, and w are the position, velocity, and remaining anaerobic energy of a cyclist. The subscripts of each parameter denote each cyclist's ID number. The state d represents the distance gap between the cyclists. The input variables to the system are the applied power of each cyclist,

$$u = \begin{bmatrix} p_1 & p_2 \end{bmatrix}^T \tag{4.6}$$

Using the individual cyclist dynamics from Chapter 3 and assuming 100%

efficiency for the bicycle's powertrain, we can write the state-space equations as,

$$\underbrace{\begin{bmatrix} \dot{s_1} \\ \dot{v_1} \\ \dot{w_1} \\ \dot{d} \\ \dot{v_2} \\ \dot{w_2} \end{bmatrix}}_{\dot{x}} = \underbrace{\begin{bmatrix} v_1 \\ \frac{1}{m_{1_{eff}}} \left(\frac{p_1}{v_1} - m_1 g \sin\theta(s_1) - m_1 g C_R \cos\theta(s_1) - 0.5 \rho A_1 C_D(-d) v_1^2 \right) \\ \mathcal{P}_1 - CP_1 \\ v_1 - v_2 \\ \frac{1}{m_{2_{eff}}} \left(\frac{p_2}{v_2} - m_2 g \sin\theta(s_2) - m_2 g C_R \cos\theta(s_2) - 0.5 \rho A_2 C_D(d) v_2^2 \right) \\ \mathcal{P}_2 - CP_2 \end{bmatrix}}_{f(x,u)} \tag{4.7}$$

where m is the bicycles total mass, m_{eff} is the effective mass of the bicycle, θ is the road angle, C_R is the rolling resistance coefficient, and $C_D(d)$ is the drag coefficient as a function of the distance gap to the front bicycle. The functions $\mathcal{P}_1$ and $\mathcal{P}_2$ represent the adjusted power of each cyclist from Equation (4.2) considering their individual model parameters.

The C_D function is an essential part of the state-space equations that can trigger the need for performing a take-over maneuver. To develop this function, it is useful to inspect the distance gap between the bicycles.

Considering the bicycles as point particles, the distance gap between the two cyclists follows,

$$\dot{d} = v_1 - v_2 \tag{4.8}$$

Therefore, when d is positive, the first cyclist is leading, and if it is negative, the second cyclist is leading. Combining the curves for leading and trailing cyclists in Figure 4.2, we can develop a drag coefficient function that outputs the trailing

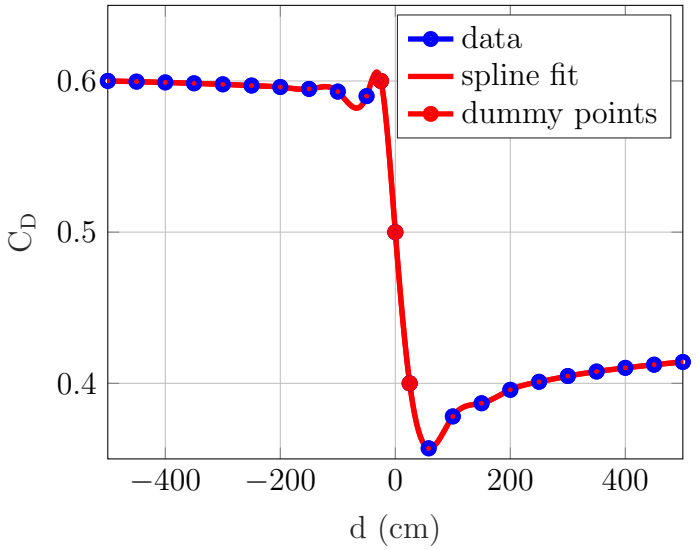

Figure 4.4: The modified drag coefficient plot for the leading and the trailing cyclists in a two-cyclist team as a function of the distance gap between the cyclists. The data is from [4]

bicycle's C_D when d is positive, and the leading bicycle's C_D when d is negative. The challenge is now implementing a minimum distance gap constraint to ensure a reasonable minimum gap between the two cyclists,

$$|d| \geqslant d_{min} \tag{4.9}$$

where d_{min} is a positive minimum gap between the bicycles. Directly imposing this constraint in the optimal control problem, prohibits the distance gap to take any value between $-d_{min}$ and $+d_{min}$. In a smooth take over maneuver, the distance should gradually go to zero and then change sign. To make this transition happen, we propose an indirect method to enforce the constraint. First, we set $d_{min} = 50$ cm as the minimum safe gap allowed between the bicycles. Then, we modify the drag coefficient when -50 $< d <$ 50 so that the drag coefficient takes larger values in this interval as shown in Figure 4.4 compared to its value at 50 cm. The red points in this figure represent the dummy point we added in the -50 $< d <$ 50 interval. This

modification incentivizes riding outside of the 50 cm gap zone. The spline fitted to the curve in Figure 4.4 is intended to capture drag coefficient function in the optimal control formulation. In this figure we can observe that if the trailing cyclist (for which $d > 0$) rides at a distance less than 50 cm the drag coefficient will be higher than when riding a 400 cm distance. Therefore, the controller is expected to avoid riding in that region. It should be noted that this does not guarantee the constraint in Equation (4.9). Applying the method described serves as a soft constraint on the distance gap.

Similar to the individual time trial case, the cost of the optimal control problem is time. We need to decide which cyclist's time should be minimized. In a two-cyclist time trial the time of the second cyclist passing the finish line will be the team's record. Therefore, it is not logical for one of the cyclists to finish significantly sooner than the other team mate. Also, during numerical simulation, similar to the DP formulation for individual time trial, we consider position as the independent variable. The position's increment is set to be 10 m. The length of the team platoon is the sum of the bicycles' lengths and the distance gap between them which will be less than 10 m during the ride. Therefore, we can minimize the average time of the team as,

$$J = \int_0^{S_f} \left(\frac{1}{v_1} + \frac{1}{v_2} \right) ds \tag{4.10}$$

where S_f is the position of the finish line. Now we can construct the optimal control problem in a formal way as,

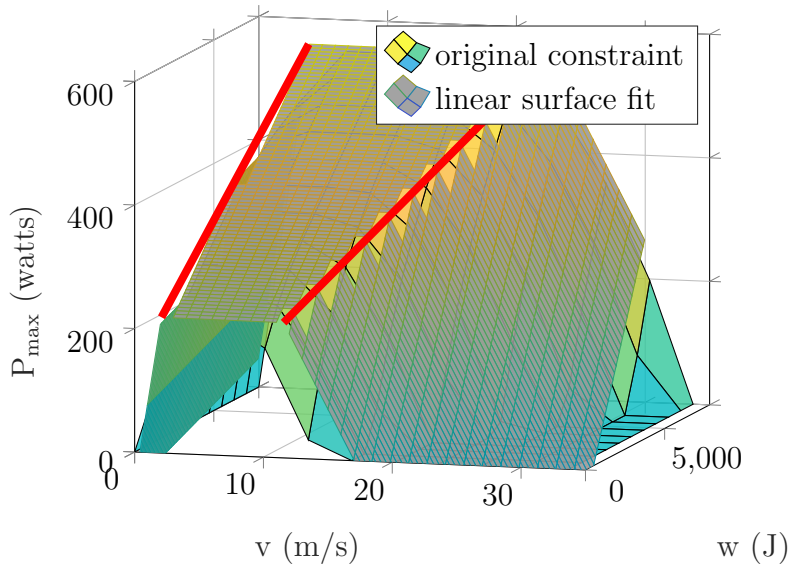

Figure 4.5: The maximum power constraint is approximated by three planes in order to reduce the number of no-linear constraints. The red lines represent the intersection of the planes.

$$\min_{u(t)} \; J = \int_0^{S_f} \left(\frac{1}{v_1} + \frac{1}{v_2} \right) ds$$

subject to:

$$\begin{aligned}
&\dot{x} = f(x, u) && \\
&0 \leqslant v_i \leqslant 20\tfrac{m}{s} && i = 1, 2 \\
&0 \leqslant w_i \leqslant AWC_i && i = 1, 2 \\
&0 \leqslant p_i \leqslant p_{i,max}(v_i, w_i) && i = 1, 2 \\
&v_i(0) = 0 && i = 1, 2 \\
&w_i(0) = AWC_i && i = 1, 2
\end{aligned} \tag{4.11}$$

The maximum power constraint $p_{i,max}(v_i, w_i)$ is derived using the same method presented in Chapter 2 and shown in Figure 3.2. In order to reduce the number of non-linear constraints in the problem, we can approximate this surface by three planes as in Figure 4.5. As a result, we will have three linear constraints instead of a single

highly non-linear one which will reduce the computation time of the optimization.

4.2.2 The Numerical Optimization

A problem, similar to our TTT formulation, that is designed to find a trajectory that optimizes an objective function, is called Trajectory Optimization. In trajectory optimization, the dynamic system's equations are transformed into a set of static equations to be solved using an optimization solver.There are several methods to do this including single shooting, multiple shooting, direct collocation, orthogonal collocation, and pseudospectral [87]. In this study we utilize the "Direct Multiple Shooting (DMS)" method which was first presented as a solution for optimal control problems in [88].

In this method, the problem formulation in Equation (4.11) is first discretized over N control time intervals. Then, we will have $u_1, u_2, ..., u_N$ each as a decision variable to be determined by the optimizer instead of having a continuous functions for u. In a similar way, we will have the states $x_1, x_2, ..., x_{N+1}$ as our decision variables. Therefore, in total we have $2N + 1$ decision variables. So far these variables are independent. To apply the system dynamics to the problem and establish the relationship between the variables, at each time step $t = k$ we need to integrate the state-space equations $f(x_k, u_k)$ to approximate x_{k+1}. There are different ways to perform the integration. The simplest method is the explicit Euler integration $x_{k+1} \approx x_k + \Delta t f(x_k, u_k)$, with $\Delta t = \frac{T}{N}$ being the time step. A more accurate method of integration that we use in the current work is the classical Runge-Kutta method (RK4),

$$x_{k+1} = x_k + \frac{\Delta t}{6}(k_1 + 2k_2 + 2k_3 + k_4) \tag{4.12}$$

where

$$\begin{aligned} k_1 &= f\left(x_k, \quad u_k\right) \\ k_2 &= f\left(x_k + k_1 \tfrac{\Delta t}{2}, \quad u_k\right) \\ k_3 &= f\left(x_k + k_2 \tfrac{\Delta t}{2}, \quad u_k\right) \\ k_4 &= f\left(x_k + k_3 \Delta t, \quad u_k\right) \end{aligned} \tag{4.13}$$

The parameters k_1 to k_4 are the slopes at four points from the start of the interval to the end. The state x_{k+1} is then calculated using a weighted sum of these slopes. We now can add Equation (4.12) as a constraint to our optimization problem. Therefore, we can write the optimal control problem presented in Equation (4.11) as an optimization problem,

$$\min_{u_1,\ldots,u_N,x_1,\ldots,x_{N+1}} T$$

$$\begin{aligned} &\text{Subject to:} \\ &x_{k+1} = x_k + \tfrac{\Delta t}{6}(k_1 + 2k_2 + 2k_3 + k_4) \quad k \in \{1, 2, ..., N\} \\ &x_{min} \leqslant x_k \leqslant x_{max} \\ &0 \leqslant u_k \leqslant u_{max}(x_k) \end{aligned} \tag{4.14}$$

where x_{min}, x_{max}, and u_{max} are vectors that include the minimum and maximum constraints on each state and control variable. The resultant optimization is a non-linear programming problem because of the non-linearity in state equations and the cost function.

For the case of two-cyclist team, we considered position as the independent

variable rather than time. Therefore, we need to write the cost function as,

$$T = \sum_{i=1}^{N+1} \left(\frac{1}{v_1} + \frac{1}{v_2} \right) \Delta s \tag{4.15}$$

where $v_1(i)$ and $v_2(i)$ represent the velocity of both cyclists at time step i. In this study we use the CasADi optimal control solver [71]. CasADi is an open source tool that helps the user implement various numerical methods of trajectory optimization for non-linear systems. It also embeds several non-linear programming (NLP) solvers such as IPOPT, BONMIN, Knitro, SNOPT, etc. For the purpose of solving the current optimization problem, IPOPT is chosen as the NLP solver [89].

The downside of employing DMS method for a nonlinear system is that the resulting non-linear programming problem can be non-convex. Therefore, we may converge to a local optimum rather than the global using the NLP solvers. This is in contrary to the Dynamic Programming that always guarantees the global optimal solution. In Chapter 3, we used Dynamic Programming for the problem of individual time trial. However, applying DP to the current problem for team time trial will be very costly in terms of computation with twice as many state and control variables as in individual time trial case. Solving the NLP from the direct multiple shooting method is a lot faster than DP, and seems to be among few viable choices that we have.

4.2.3 Simulation Results

The two cyclists in this case study have distinct fatigue and recovery model parameters which are presented in Table 4.1. Cyclist #1, who is Sub 14 from our list of subjects for experiments, is a stronger athlete with a higher CP, AWC, and maximum cadence $\omega_{max,f}$ compared to the other rider. On the other hand, the parameters

Table 4.1: Model parameters of the cyclists in the two-cyclist team case study.

	cyclist #1	cyclist #2
mass (kg)	82	70
CP (watts)	242	217
AWC (J)	7841	5637
a	0.08	0.12
b (watts)	222.5	196.5
α	0.044	0.046
α_ω	0.008	0.009
$\omega_{max,f}$ (rpm)	164	142

for the cyclist #2 are those from Sub 12 who has a faster recovery rate than the other cyclist. The elevation profile used in this simulation is the same 2019 National Duathlon Championship course in Greenville, SC that was presented in the individual time trial simulation presented in Chapter 3.

The simulations in MATLAB using IPOPT was performed on a Dell desktop computer with a 2.9 GHz 10^{th} generation Intel Core i7 CPU, and 12GB of RAM and took an hour to complete. The simulation results are presented in Figure 4.6. The results show that despite having a very similar velocity trajectory, the cyclists have fundamentally different energy expenditure strategies. Cyclist #1 is consistent in applied power, without much fluctuation, which results in a gradual decrease of the remaining anaerobic energy. On the other hand, the power of cyclist #2 frequently varies over time. When in the leading position this cyclist applies high power and burns a considerable amount of anaerobic energy. Then, by switching positions, #2 drafts behind #1 and recovers a significant portion of the lost energy.

For understanding the reason behind the large recovery sections for cyclist #2, the distance gap plot in Figure 4.6 can be inspected. When d is positive, cyclist #1 is leading, and when it is negative, cyclist #2 is leading. It can be seen that for a larger portion of the ride, cyclist #1 is leading who is the stronger athlete. Therefore,

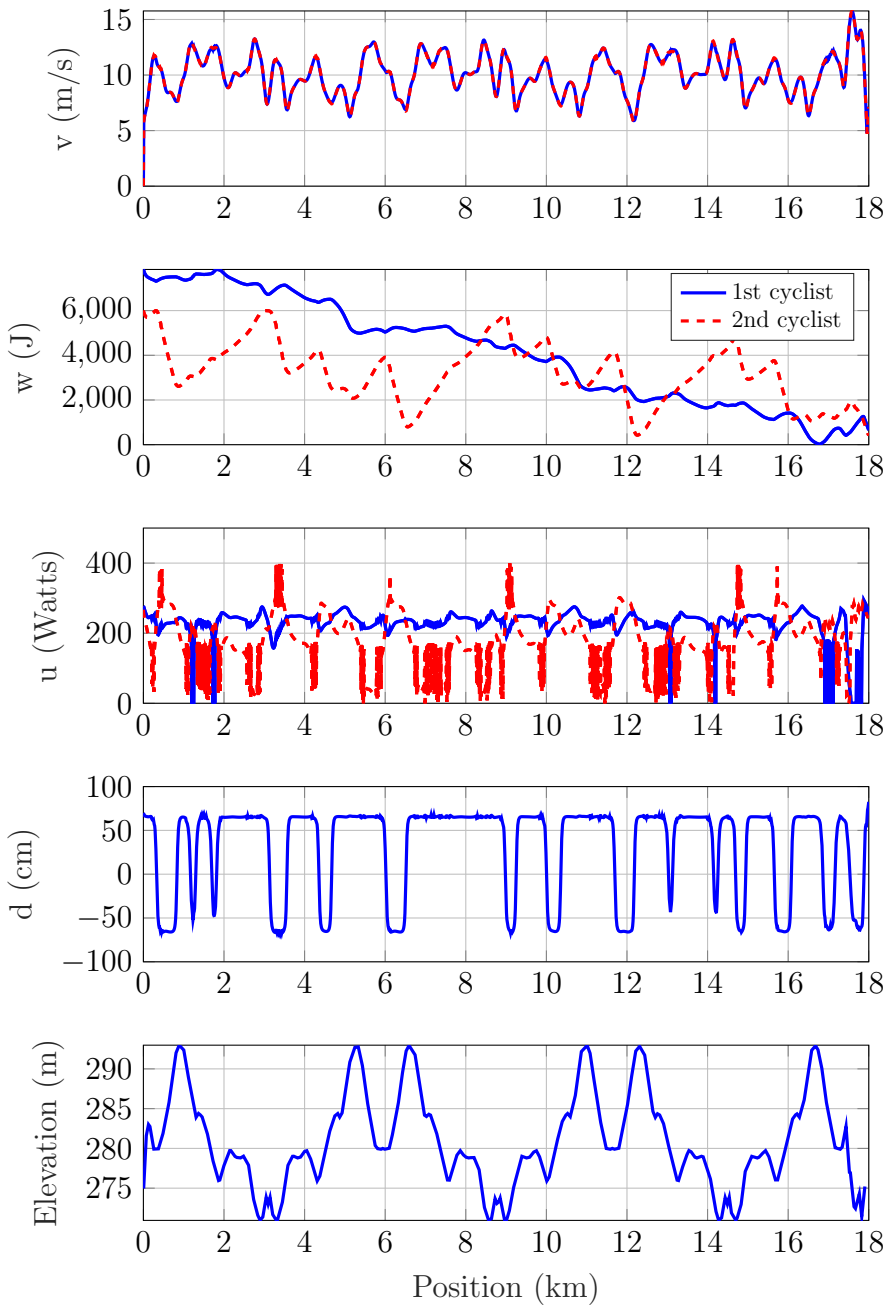

Figure 4.6: Simulation results for a two-cyclist team riding over the 2019 Duathlon National Championship in Greenville, SC.

cyclist #2 has the opportunity to recover for larger time durations.

As a baseline for comparison, we ran the optimization a second time by imposing a hard constraint for the distance gap to be always positive. In other words, a case where the cyclists do not switch positions, and cyclist #1 is always in the lead. The results of this baseline simulation is shown in Figure 4.7. The team time record in the baseline simulation was 1969 seconds, and in the optimal simulation was 1880 seconds, which shows a 4.7% reduction in travel time when the cyclists switch positions. By comparing the energy expenditures of the cyclists in the baseline and the optimal simulations, we can observe that cyclist #2 recovers a lot more anaerobic energy in the optimal simulation, which enables the cyclist to generate higher power levels.

An important take away from this case study is that the distance gap between the cyclists switches between +57cm and −57cm which are the corresponding distance gaps for the minimum drag coefficient in leading and trailing positions according to the plot in Figure 4.4. Therefore, if we assume that the cyclists can switch positions instantly, we can fix the distance gap at the minimum possible. Then, a binary decision variable can be considered as a decision variable that commands a take over maneuver when necessary. This result is specially helpful for developing the formulation for a general n-cyclist team.

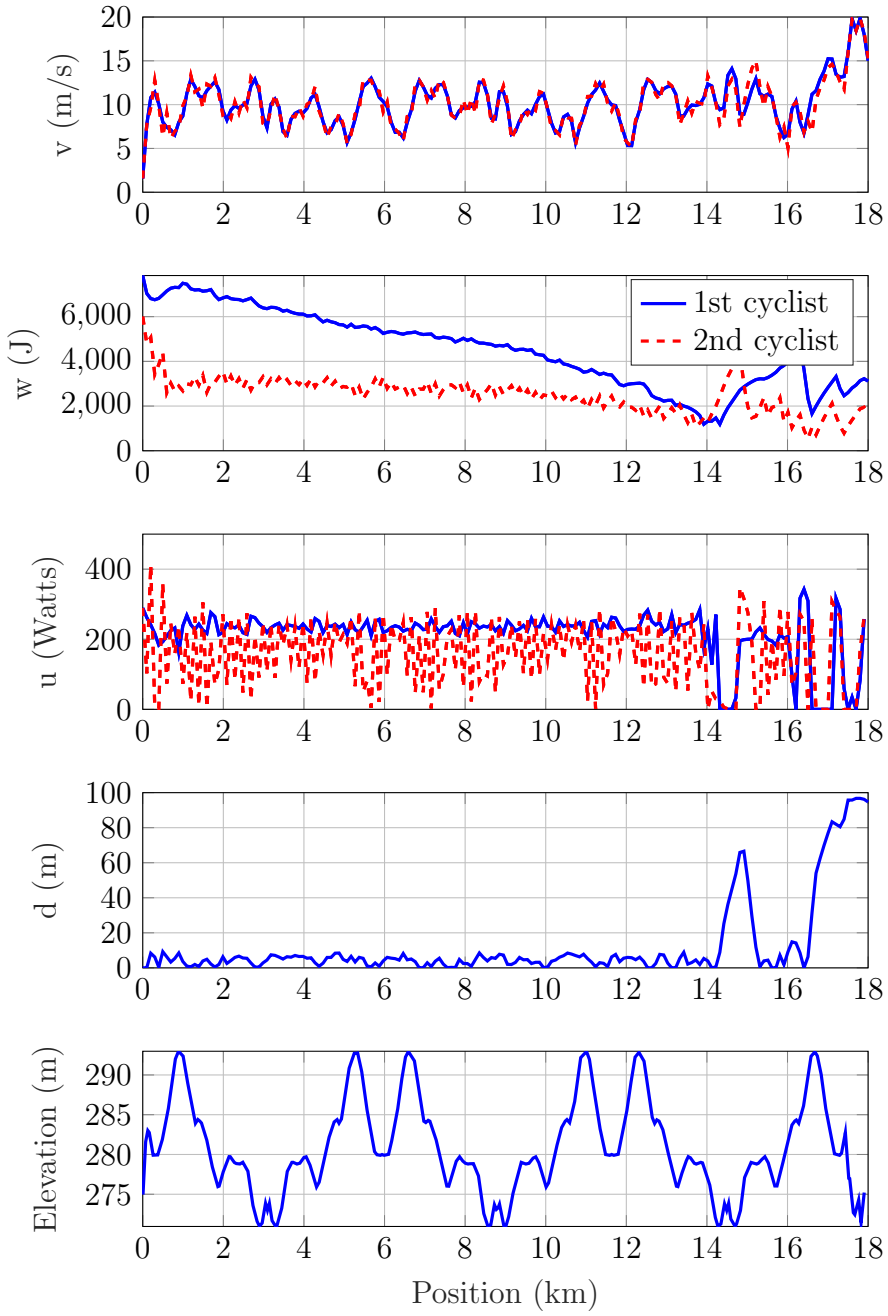

Figure 4.7: Baseline simulation results for a two-cyclist team without switching positions.

4.3 n-Cyclist Team

4.3.1 Problem Formulation

Our takeaway from the two-cyclist team case study is that the distance can be fixed at the minimum safe value. We utilize this fact when formulating the formation optimization problem for an n-cyclist team. There are two more assumptions we make for this problem. First, in an n-cyclist team, the time of the n^{th} rider passing the finish line will be the team's record. This is not the case for several TTT competitions. For instance, in the TTT stage of the Tour de France, for a six-cyclist team, the finish time of the 4^{th} cyclist is the team's record. Second, the cyclists can switch their positions in the platoon instantaneously. In other words, we neglect the dynamics of the overtaking maneuver, and assume that during each maneuver, cyclists do not expend any energy. With these simplifying assumptions, we conclude that the velocity and acceleration of all cyclists should be the same to maintain a constant distance with each other. Therefore, instead of the velocity of each cyclist, we consider the platoon velocity as a state variable, in addition to the platoon head position s,

$$\begin{aligned} \dot{s} &= v_p \\ \dot{v_p} &= u_a \end{aligned} \tag{4.16}$$

where v_p is the platoon velocity and u_a is the acceleration of the platoon which we consider as a control input. Additionally, from Equation (4.3) the dynamics of the remaining anaerobic energy of each cyclist is,

$$\dot{w_i} = \mathcal{P}_i - CP_i \quad \text{for} \quad i = 1, 2, ..., n \tag{4.17}$$

Since we consider the platoon acceleration u_a as a control input, we should

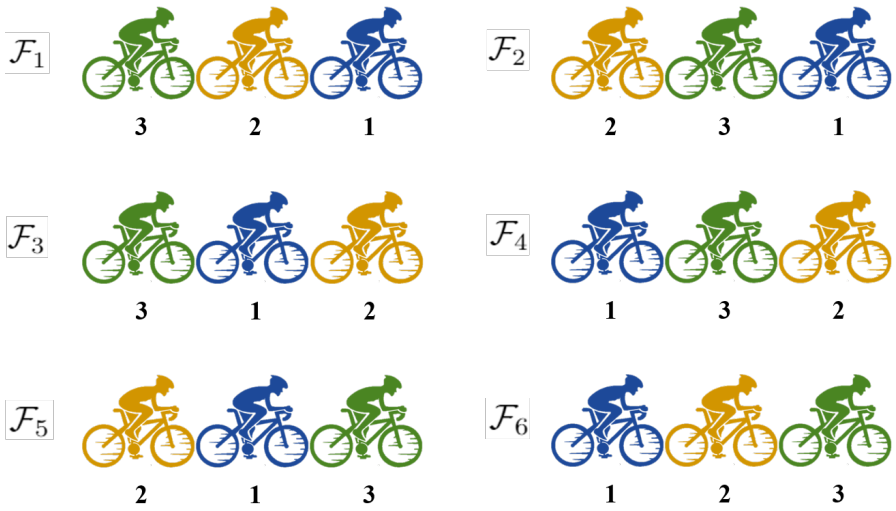

Figure 4.8: All 6 formations in a three-cyclist team.

calculate each subject's power p_i from acceleration, velocity, and position within the platoon,

$$p_i = v_p \left(m_{i_eff} u_a + m_i g \sin\theta(s) + m_i g C_R \cos\theta(s) + 0.5 \rho A_i C_{D_i} v_p^2 \right) \tag{4.18}$$

where C_{D_i} is the drag coefficient for each cyclist depending on his or her position in the platoon. In order to determine the position of the cyclists in the platoon, we propose a method that includes a vector of binary decision variables. For an n-cyclist team, there are n factorial distinguished formations. For example, there are six possible formations for a team of three cyclists as shown in Figure 4.8.

Let's assign to each formation a binary variable indicating whether the team is currently in that specific formation or not,

$$\mathcal{F}_j \in \{0, 1\} \quad \text{for} \quad j = 1, 2, ..., n! \tag{4.19}$$

where $\mathcal{F}_j$ is 1 when the formation j is selected. Figure 4.8 shows each $\mathcal{F}_j$ assigned to a unique formation. Since at every point in time only one formation can exist, we add the following constraint,

$$\sum_{j=1}^{n!} \mathcal{F}_j = 1 \tag{4.20}$$

Each $\mathcal{F}_j$ serves as a decision variable that is to be determined by the optimal controller.

For every formation the drag coefficient of the cyclists in the platoon is known from Figure 4.3, which suggests the drag coefficients for a cyclist in the first, second, and third position in the team are 0.59, 0.38, and 0.31, respectively. If we construct a vector of the corresponding drag coefficients for each cyclist with respect to every formation $\mathcal{F}_j$, we can calculate C_{D_i} for the cyclists in a team of three as,

$$\begin{aligned}
C_{D_1} &= \begin{bmatrix} \mathcal{F}_1 & \mathcal{F}_2 & \mathcal{F}_3 & \mathcal{F}_4 & \mathcal{F}_5 & \mathcal{F}_6 \end{bmatrix} \begin{bmatrix} 0.59 & 0.59 & 0.38 & 0.31 & 0.38 & 0.31 \end{bmatrix}^T \\
C_{D_2} &= \begin{bmatrix} \mathcal{F}_1 & \mathcal{F}_2 & \mathcal{F}_3 & \mathcal{F}_4 & \mathcal{F}_5 & \mathcal{F}_6 \end{bmatrix} \begin{bmatrix} 0.38 & 0.31 & 0.59 & 0.59 & 0.31 & 0.38 \end{bmatrix}^T \\
C_{D_3} &= \begin{bmatrix} \mathcal{F}_1 & \mathcal{F}_2 & \mathcal{F}_3 & \mathcal{F}_4 & \mathcal{F}_5 & \mathcal{F}_6 \end{bmatrix} \begin{bmatrix} 0.31 & 0.38 & 0.31 & 0.38 & 0.59 & 0.59 \end{bmatrix}^T
\end{aligned} \tag{4.21}$$

where C_{D_1}, C_{D_2}, and C_{D_3} are the drag coefficients in Equation (4.18). With the proposed formulation the velocity of all cyclists are equal. Therefore, to write the cost of this optimal control problem we consider the completion time of the platoon as the variable to be minimized. Similarly to the two-cyclist case study in Section 4.2.1 the position interval is considerably larger than the length of the platoon. Thus, minimizing the time of the platoon means minimizing the last cyclist in the team as well. We can now construct the optimal control problem as,

$$\min_{u_a(t),\mathcal{F}_j(t)} \quad J = \int_0^T dt$$

$$\begin{aligned}
&\text{Subject to:} \\
&\dot{s} = v_p \\
&\dot{v_p} = u_a \\
&\dot{w_i} = \mathcal{P}_i - CP_i && i = 1, 2, ..., n \\
&\textstyle\sum_{j=1}^{n!} \mathcal{F}_j(t) = 1 && j = 1, 2, ..., n! \\
&0 \leqslant v_p \leqslant 20\tfrac{m}{s} \\
&0 \leqslant w_i \leqslant AWC_i \\
&0 \leqslant p_i \leqslant p_{i,max}(v_p, w_i)
\end{aligned} \tag{4.22}$$

where $p_{i,max}$ is the maximum power constraint from Figure 4.5. Unlike the previous cases for individual time trial and two-cyclist team trial, we consider time t as the independent variable. CasADi has a collection of helper classes called "Opti" that can be used to translate an optimal control formulation to a non-linear programming optimization. Opti stack provides the ability to define final time as the optimization objective, and consider time as the independent variable. Therefore, we used Opti to keep the formulation as is in Equation (4.22).

4.3.2 Simulation and Results

The three cyclists selected for this simulation are Sub 14, Sub 12, and Sub 9 for whom we have experimental data. Their model parameters are presented in Table 4.2. The elevation profile considered for this case is from the first 10 km of the 2019 National Duathlon Championship in Greenville.

As shown in Figure 4.8, there will be six binary decision variables representing

Table 4.2: Model parameters of the cyclists in the two-cyclist team case study.

	cyclist #1	cyclist #2	cyclist #3
mass (kg)	82	70	63
CP (watts)	242	217	233
AWC (J)	7841	5637	10100
a	0.08	0.12	0.09
b (watts)	222.5	196.5	204.5
α	0.044	0.046	0.036
α_ω	0.008	0.009	0.014
$\omega_{max,f}$ (rpm)	164	142	158

all the formations of cyclists in the platoon. Applying the same direct multiple shooting method presented in Section 4.2.2, the resultant optimization problem will be of a mixed-integer non-linear programming (MI-NLP) form. We chose the Bonmin solver for the optimization which is designed for MI-NLP type problems [90], and uses the Branch-and-Bound (BB) method. While applicable for other types of problems, the BB method is widely used for MI-NLP optimization [91].

It should be noted that utilizing the BB method, especially when applied to a problem with multiple integer variables, can be computationally costly. In the worst case, the method is exponential in terms of time complexity. In our specific problem for a three-cyclist team, after constructing the MI-NLP optimization problem using the direct multiple shooting method, we will have $6 \times N$ binary decision variables, assuming N control intervals. Therefore, by increasing N, the simulation time gets exponentially higher.

To avoid long simulation time, we divide the simulation into two parts. First, we run the optimization by setting the number of control intervals at $N = 50$. From the results of this simulation we obtain the optimal formation trajectory of cyclists as shown in Figure 4.9. It can be seen in this figure that the cyclists have tried all of the possible formations from $\mathcal{F}_1$ to $\mathcal{F}_6$. Additionally, it is important to note

that the formations selection is not based on the remaining anaerobic energy of the cyclists. This means, a cyclist with the highest anaerobic energy is not necessarily in the leading position.

However, for a 10 km course with 50 control intervals, the distance interval for receiving a formation command will be on average 200 m which is significantly larger than our previous distance interval of 10 m in the two-cyclist team case study. That is why the velocity, anaerobic energy, and acceleration plots in Figure 4.9 have low resolutions. Thus, we run the optimization a second time with $N = 200$, and by fixing $\mathcal{F}_j$ at the values obtained from the simulation with $N = 50$ control intervals. Since the binary variables $\mathcal{F}_j$ are known, the new optimization problem will not include any integer decision variable with platoon acceleration as the only control input as represented in Equation (4.23). To emphasize the difference in time complexity, it should be noted that the resultant MI-NLP simulation with $N = 50$ took 8 hours and 10 minutes, while the NLP simulation with $N = 200$ took 30 seconds.

$$\min_{u_a(t)} \; J = \int_0^T dt$$

$$\begin{aligned}
&\text{Subject to:} \\
&\dot{s} = v_p \\
&\dot{v_p} = u_a \\
&\dot{w_i} = \mathcal{P}_i - CP_i \qquad\qquad i = 1, 2, ..., n \\
&0 \leqslant v_p \leqslant 20\tfrac{m}{s} \\
&0 \leqslant w_i \leqslant AWC_i \\
&0 \leqslant p_i \leqslant p_{i,max}(v_p, w_i)
\end{aligned} \tag{4.23}$$

The downside of this two-step optimization is that the final result is not nec-

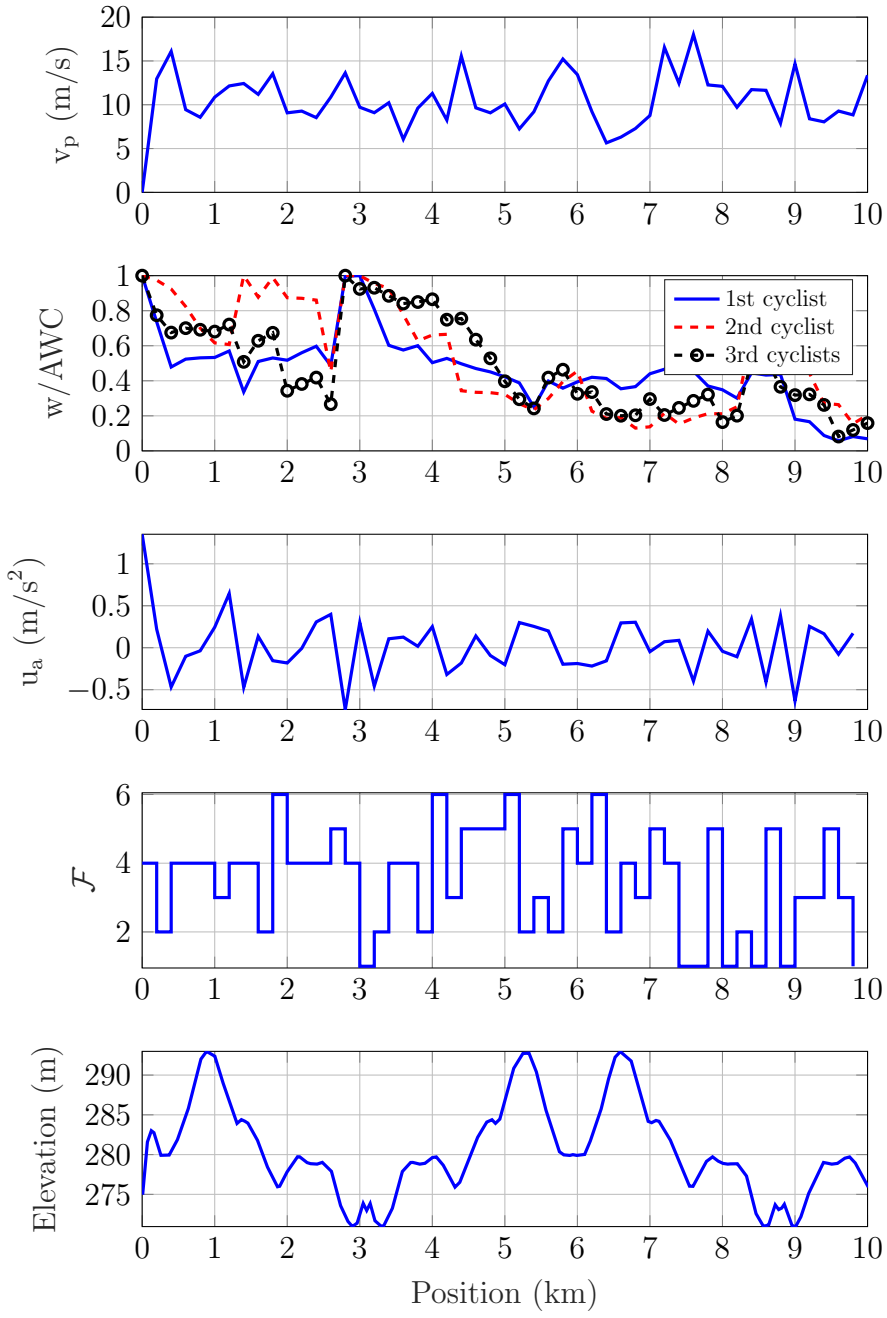

Figure 4.9: Simulation results for a three-cyclist team riding over the first 10 km of the 2019 Duathlon National Championship in Greenville, SC. This result is for the case with 50 control intervals. We save the optimal formation trajectory to be used later in the higher resolution simulation.

essary the same as a one-step MI-NLP optimization with $N = 200$. The results of the simulation with optimal formation are presented in Figure 4.10. The results in this figure show that there is no rule based relationship between the optimal formation and the remaining anaerobic energy of each cyclist. In other words, the cyclists are not sorted based on how much anaerobic energy they have at the time. Therefore, there is a necessity to perform the mathematical optimization for each competition with its unique elevation profile.

In order to determine the effectiveness of the formation trajectory decided by the controller, a baseline simulation is required. The universal strategy for cyclists in a team time trial race is that the team members alternatively take the lead which is called " taking a pull" [4]. Then, after a set time interval in the lead position, a cyclist goes to the back of the line. Although this is a practical and easy to perform strategy, it is rule based and not necessarily mathematically optimal.

To simulate the baseline case, we first construct the formation trajectory for $N = 50$ control intervals assuming that at the end of every control interval the lead cyclist goes to the back of the platoon. According to Figure 4.8, if the team starts at formation $\mathcal{F}_1$, the team's formation will be $\mathcal{F}_4$ for the next interval, and after that $\mathcal{F}_5$. Then, the same order is repeated. Once we set the formation trajectory, we solve the optimal control problem in Equation (4.23). This way, the only difference between the baseline and the optimal formation simulation is the formation strategy.

The baseline simulation results are presented in Figure 4.11. The team's finish time in the baseline test was found to be 912.4 sec, while in the simulation with the optimal formation this time was 881.3 sec which shows %2.3 reduction in travel time. The most important conclusion from comparing these two results is that the current general strategy that is being practiced in time trial teams is not optimal. In fact, we observe in Figure 4.10 that all possible formations from $\mathcal{F}_1$ through $\mathcal{F}_6$ are adopted

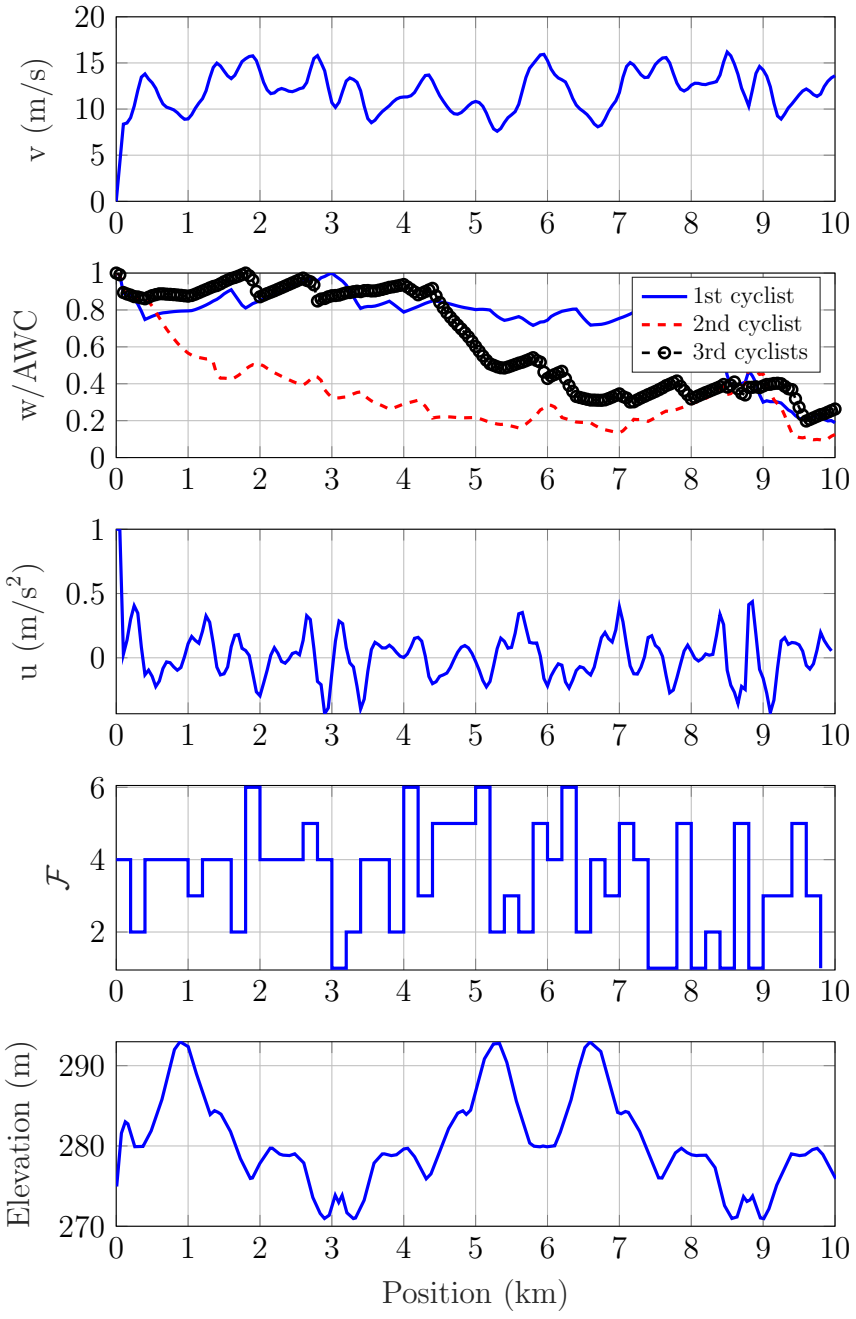

Figure 4.10: Simulation results for a three-cyclist team riding over the first 10 km of the 2019 Duathlon National Championship in Greenville, SC. This result is ran with 200 control intervals and the formation trajectory from Figure 4.9

during the trial.

In practice, the fatigue and recovery model parameters of each team member should be determined. Then, the proposed optimization simulation should be conducted prior to the competition to derive the optimal formation strategy during the race. Practice with the optimal formation can help the cyclists adapt to the strategy and be able to follow it during the competition.

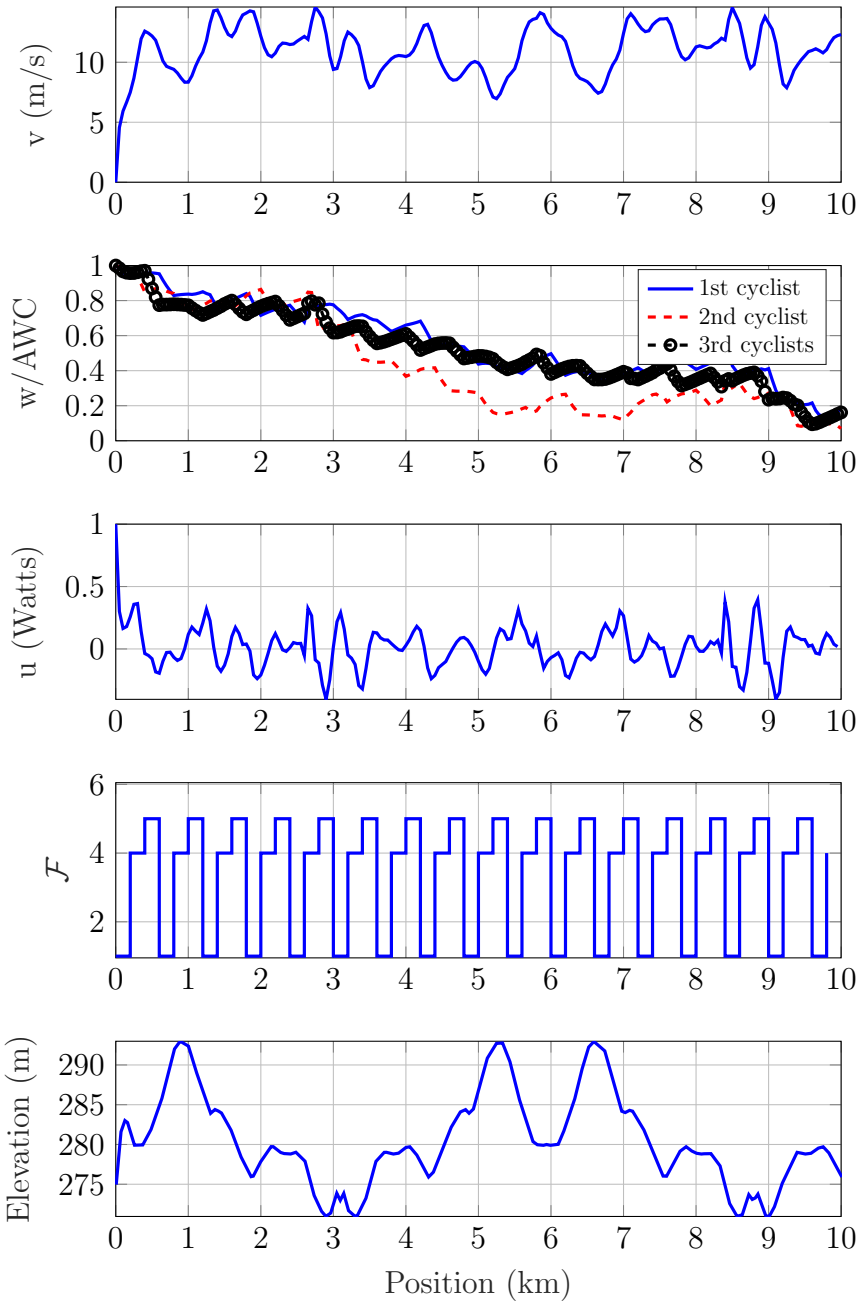

Figure 4.11: The baseline simulation results for a three-cyclist team.

4.4 Conclusion

In a Team Time Trial (TTT) competition, cyclists of a team form a platoon by riding in close distance between each other, which is called drafting. Drafting can help significantly reduce the aerodynamic drag coefficient on the trailing cyclists. In this chapter, using the individual models of fatigue and recovery presented in Chapter 2, a novel optimal control formulation is proposed that decides how and when the cyclists should change their position in the platoon. As a case study, we first formulated the problem for a two-cyclist team. The elevation profile of the 2019 National Duathlon Championship in Greenville, SC was selected for the simulation. The optimization was solved using the commercial solver CasADi. According to the simulation results, the time record of the team was reduced by 4% when the cyclists optimally switched their positions compared to a baseline case where the cyclists formation was unchanged during the race. Another observation form this simulation was that during the intervals where cyclists did not switch positions, their distance remained at the minimum safe gap.

We then expanded the formulation to an n-cyclist team where the finishing time of the n^{th} cyclist is considered as the team record. Since in the two-cyclist case study we showed that the optimal distance gap between the cyclists is fixed, we did not consider distance as a state variable in the formulation and set it as a constant. Because the distance gap was constant between the cyclists, their velocity was the same. Therefore, instead of having three separate state variables for velocity of each cyclist, the velocity of the platoon was considered as a state variable. The control variables in this formulation were the formation of cyclists in the platoon and the platoon acceleration. The simulation results for a three-cyclist team over the first 10 km of the 2019 National Duathlon Championship course, showed a 2.3% reduction in

travel time compared to a baseline simulation. The baseline simulation was designed using a widely practiced strategy by professional cycling teams. In this rule-based strategy, the cyclist in the leading position goes to the back of the platoon at the end of the time interval. This process is repeated by all of the cyclists in the platoon. From the simulation results, we conclude that the formation strategy of a team depends on the conditions of a specific race, and applying a rule-based general strategy is not necessarily optimal for every competition.

Chapter 5

Conclusions

Optimal pacing of a cyclist in a time-trial was formulated as an optimal control problem with an emphasis on the influence of depletion and recovery of anaerobic reserve on performance. In particular each cyclist's maximal power varies with level of fatigue and chosen cadence and plays a critical role in determining the optimal pace in a hilly time-trial. To that end, state-space dynamic models that track depletion and recovery of Anaerobic Work Capacity (AWC) as a function of rider's power above or below their Critical Power (CP) were hypothesized and were validated and calibrated using data from six human subject tests after each spent 14 hours in the lab. In addition, a model was obtained from experimental data relating cyclists' maximal power to their remaining anaerobic capacity and their cadence. With the models in place, we were able to usefully employ Pontryagin's Minimum Principle, and that over any road profile, the optimal strategy is bang-singular-bang, switching between maximum exertion, no exertion, pedaling at CP, or cruising at constant speeds. Once global optimality was confirmed, limiting the quantization of the cyclist power to only these four optimal modes, substantially reduced the computational load of DP and allowed finer quantization of the states. We demonstrated that the strategy for an

18 km course can be computed in around 2 minutes, well below what was needed in a standard DP implementation.

Simulations over simple road profiles with one or two steep climbs, showed the efficacy of the optimal strategy in distributing the depletion of AWC along the whole course and appropriately pacing the cyclist in anticipation of climbs. We also simulated human subject 14 over the 2019 Greenville Duathlon course. We had data from subject 14 pedaling the same course on a CompuTrainer with her self-strategy. The simulation suggested that optimal pacing could speed up subject 14 and allow her to finish the course in 76% of her original time (reduction from 2048 seconds to 1556 seconds) with a 28 Watt increase in her average output power which is 11% of her CP. The comparison indicates that consistency in power generation is a key difference between the subject's self and the optimal strategies. While the power should be kept at CP for most of the ride, the cyclist benefits from frequent short sprints to increase velocity.

We have also set up a test protocol using a CompuTrainer for providing optimal power to our subjects in real time, and to observe their performance improvement in laboratory environment. At the time of writing this dissertation, unfortunately we were forced to pause our human subject testing because of the spread of COVID-19. We had the opportunity to perform a pilot test before the pandemic in which we observed about 3% improvement in travel time when the subject followed the optimal power to hold provided by the controller compared to the subject's self-strategized pace.

In addition to the individual time trial competition, we expanded our work to study the team time trial (TTT). During this type of competitions the cyclists in the trailing positions benefit from a rather significant reduction in the aerodynamic drag force by riding in a close distance to their preceding teammates. The current

general strategy of the professional cycling team during a TTT race is that the team members alternatively take the lead. Then, after spending a single time interval in the lead position, the lead cyclist goes to the back of the line. We first formulated an optimal control problem for a case study involving a two-cyclist team using the previously calibrated models of fatigue and recovery for two of our subjects. Using the direct multiple shooting method, the optimal control problem was transcribed into a non-linear programming problem which was solved using CasADi solver. The case study showed that the distance between the cyclists can be fixed at its minimum safe value. That means we only need to determine the formation of the cyclists in the team.

Next, we developed a generalized formulation for an n-cyclist team where their formation is determined using n factorial binary decision variables in addition to velocity and acceleration of the entire platoon decision choices. This leads to a mixed-integer non-linear programming problem. We then simulated a 10 km time trial race for a three-cyclist team. Since having several binary decision variables significantly increases the computation time, we first ran a low resolution simulation with 50 control intervals. From this trial, the optimal formation trajectory was saved and fed to a second optimization trial with 200 control intervals. In the second simulation, the only control input was acceleration since formation trajectory is fixed. To examine the effectiveness of the controller, we also ran a baseline simulation using the rule-based strategy where the lead cyclist goes to the back of the line periodically. The results show 2.3% reduction in travel time for the optimal formation simulation compared to the baseline. This confirms that the current well known rule-based formation strategy has room for improvement. For an optimal performance, a cycling team needs to perform the mathematical optimization prior to a competition to find and practice the prescribed formation strategy.

In summary, the contributions of this dissertation are:

- Proposing a novel set of dynamic models of athletes' fatigue and recovery which are validated using experimental data.
- Formulating an individual time trial race as an optimal control problem and solving it both analytically and numerically. The simulation results show 24% reduction in travel time compared to a baseline experiment where the subject followed her own strategy.
- Implementing the controller in action and providing power suggestion to a cyclist pedaling on a CompuTrainer over a simulated elevation profile in the laboratory environment. To the best of the authors knowledge, this is the first try for implementing a controller to pace a cyclist during a time trial.
- Expanding the optimal control formulation for a team time trial race, and simulations for a two-cyclist and a three-cyclist team. We confirm that the current widely used strategy, where the lead cyclists periodically goes to the back of the platoon, has room for improvement via mixed-integer NLP. The formation strategy depends on the elevation profile of each race, as well as the fatigue and recovery model parameters for the team members.

There is still much opportunity for future work. Most importantly, the proposed experiment in this dissertation for real-time use of the optimal pacer in an individual time trial should be repeated with multiple subject to verify the effectiveness of implementing the controller. Given that the proposed test setup is located in a laboratory environment, the next step would be doing experiments on a real road. To enable outdoor experiment, a power sensor that can communicate real-time data to the controller is required along with an on-board communication device for sending

the measurements to a server computer that runs the controller. The controller then sends back the optimal power to hold to the cyclist.

Moreover, the Team Time Trial simulation should be done with more realistic assumptions. For instance, several TTT competitions do not consider the time of the last team member passing the finish line as the team's record. In fact for a six-cyclist team, the finish time of the fourth cyclist is considered the team's record. The optimal control formulation should be modified to consider this rule. This will not be an easy task because it will likely results in an increasing number of state variable in the formulation, which will make it computationally expensive to solve.

Bibliography

[1] John E Hall. *Guyton and Hall textbook of medical physiology e-Book*. Elsevier Health Sciences, 2015.

[2] Jean-Benoit Morin and Pierre Samozino. *Biomechanics of training and testing: innovative concepts and simple field methods*. Springer, 2018.

[3] Pieter Abbeel. Lecture 3: Solving continuous mdps with discretization. `https://www.youtube.com/watch?v=mJlAfKc4990&ab_channel=PieterAbbeel`.

[4] Bert Blocken, Thijs van Druenen, Yasin Toparlar, Fabio Malizia, Paul Mannion, Thomas Andrianne, Thierry Marchal, Geert-Jan Maas, and Jan Diepens. Aerodynamic drag in cycling pelotons: New insights by cfd simulation and wind tunnel testing. *Journal of Wind Engineering and Industrial Aerodynamics*, 179:319–337, 2018.

[5] Chris R Abbiss and Paul B Laursen. Models to explain fatigue during prolonged endurance cycling. *Sports medicine*, 35(10):865–898, 2005.

[6] BWJJ Bigland-Ritchie and JJ Woods. Changes in muscle contractile properties and neural control during human muscular fatigue. *Muscle & nerve*, 7(9):691–699, 1984.

[7] S Alireza Fayazi, Nianfeng Wan, Stephen Lucich, Ardalan Vahidi, and Gregory Mocko. Optimal pacing in a cycling time-trial considering cyclist's fatigue dynamics. In *American Control Conference (ACC), 2013*, pages 6442–6447. IEEE, 2013.

[8] Nianfeng Wan, S Alireza Fayazi, Hamed Saeidi, and Ardalan Vahidi. Optimal power management of an electric bicycle based on terrain preview and considering human fatigue dynamics. In *American Control Conference (ACC), 2014*, pages 3462–3467. IEEE, 2014.

[9] R Hugh Morton. The critical power and related whole-body bioenergetic models. *European journal of applied physiology*, 96(4):339–354, 2006.

[10] Haley C Bergstrom, Terry J Housh, Jorge M Zuniga, Daniel A Traylor, Robert W Lewis Jr, Clayton L Camic, Richard J Schmidt, and Glen O Johnson. Differences among estimates of critical power and anaerobic work capacity derived from five mathematical models and the three-minute all-out test. *The Journal of Strength & Conditioning Research*, 28(3):592–600, 2014.

[11] Dona J Housh, Terry J Housh, and Sonja M Bauge. A methodological consideration for the determination of critical power and anaerobic work capacity. *Research Quarterly for Exercise and Sport*, 61(4):406–409, 1990.

[12] Gregory C Bogdanis, Mary E Nevill, Leslie H Boobis, HK Lakomy, and Alan M Nevill. Recovery of power output and muscle metabolites following 30 s of maximal sprint cycling in man. *The Journal of physiology*, 482(2):467–480, 1995.

[13] Faraz Ashtiani, Vijay Sarthy M Sreedhara, Ardalan Vahidi, Randolph Hutchison, and Gregory Mocko. Experimental modeling of cyclists fatigue and recovery dynamics enabling optimal pacing in a time trial. In *2019 American Control Conference (ACC)*, pages 5083–5088. IEEE, 2019.

[14] Faraz Ashtiani, Vijay Sarthy M Sreedhara, Ardalan Vahidi, Randolph Hutchison, and Gregory Mocko. Optimal pacing of a cyclist in a time trial based on experimentally calibrated models of fatigue and recovery. *arXiv preprint arXiv:2007.11393*, 2020.

[15] Vijay Sarthy M Sreedhara, Faraz Ashtiani, Gregory Mocko, Ardalan Vahidi, and Randolph Hutchison. Modeling the recovery of w' in the moderate to heavy exercise intensity domain. *Medicine and Science in Sports and Exercise*, 2020.

[16] Jenny De Jong, Robbert Fokkink, Geert Jan Olsder, and AL Schwab. The individual time trial as an optimal control problem. *Proceedings of the Institution of Mechanical Engineers, Part P: Journal of Sports Engineering and Technology*, 231(3):200–206, 2017.

[17] N. K. Vøllestad. Measurement of human muscle fatigue. *Journal of Neuroscience Methods*, 74(2):219–227, 1997.

[18] Richard HT Edwards. Human muscle function and fatigue. *Human muscle fatigue: physiological mechanisms*, pages 1–18, 1981.

[19] Roger M Enoka and Douglas G Stuart. Neurobiology of muscle fatigue. *Journal of applied physiology*, 72(5):1631–1648, 1992.

[20] Charles S Fulco, Steven F Lewis, Peter N Frykman, Robert Boushel, Sinclair Smith, Everett A Harman, Allen Cymerman, and Kent B Pandolf. Muscle fatigue and exhaustion during dynamic leg exercise in normoxia and hypobaric hypoxia. *Journal of Applied Physiology*, 81(5):1891–1900, 1996.

[21] Derek Kay and Frank E Marino. Fluid ingestion and exercise hyperthermia: implications for performance, thermoregulation, metabolism and the development of fatigue. *Journal of sports sciences*, 18(2):71–82, 2000.

[22] Derek Kay, Frank E Marino, Jack Cannon, Alan St Clair Gibson, Mike I Lambert, and Timothy D Noakes. Evidence for neuromuscular fatigue during high-intensity cycling in warm, humid conditions. *European journal of applied physiology*, 84(1-2):115–121, 2001.

[23] Craig Williams and Sébastien Ratel. *Human muscle fatigue*. Routledge, 2009.

[24] J Mark Davis and Stephen P Bailey. Possible mechanisms of central nervous system fatigue during exercise. *Medicine and science in sports and exercise*, 29(1):45–57, 1997.

[25] Jane A Kent-Braun. Central and peripheral contributions to muscle fatigue in humans during sustained maximal effort. *European journal of applied physiology and occupational physiology*, 80(1):57–63, 1999.

[26] Roger M Enoka and Jacques Duchateau. Muscle fatigue: what, why and how it influences muscle function. *The Journal of physiology*, 586(1):11–23, 2008.

[27] Joachim Liepert, Sylvia Kotterba, Martin Tegenthoff, and Jean-Pierre Malin. Central fatigue assessed by transcranial magnetic stimulation. *Muscle & Nerve: Official Journal of the American Association of Electrodiagnostic Medicine*, 19(11):1429–1434, 1996.

[28] RS Moussavi, PJ Carson, MD Boska, MW Weiner, and RG Miller. Nonmetabolic fatigue in exercising human muscle. *Neurology*, 39(9):1222–1222, 1989.

[29] Brian L Allman and Charles L Rice. Neuromuscular fatigue and aging: central and peripheral factors. *Muscle & nerve*, 25(6):785–796, 2002.

[30] Toshio Moritani, Masuo Muro, and Akira Nagata. Intramuscular and surface electromyogram changes during muscle fatigue. *Journal of Applied Physiology*, 60(4):1179–1185, 1986.

[31] Brenda Bigland and OCJ Lippold. Motor unit activity in the voluntary contraction of human muscle. *The Journal of Physiology*, 125(2):322–335, 1954.

[32] JR Potvin and LR Bent. A validation of techniques using surface emg signals from dynamic contractions to quantify muscle fatigue during repetitive tasks. *Journal of Electromyography and Kinesiology*, 7(2):131–139, 1997.

[33] Björn Gerdle, Barbro Larsson, and Stefan Karlsson. Criterion validation of surface emg variables as fatigue indicators using peak torque: a study of repetitive maximum isokinetic knee extensions. *Journal of Electromyography and Kinesiology*, 10(4):225–232, 2000.

[34] P Cerretelli, D Pendergast, WC Paganelli, and DW Rennie. Effects of specific muscle training on vo2 on-response and early blood lactate. *Journal of Applied Physiology*, 47(4):761–769, 1979.

[35] Thomas J Barstow, S Buchthal, S Zanconato, and DM Cooper. Muscle energetics and pulmonary oxygen uptake kinetics during moderate exercise. *Journal of Applied Physiology*, 77(4):1742–1749, 1994.

[36] Bengt Saltin and Soren Strange. Maximal oxygen uptake:" old" and" new" arguments for a cardiovascular limitation. *Medicine and science in sports and exercise*, 24(1):30–37, 1992.

[37] Thomas J Barstow, Andrew M Jones, Paul H Nguyen, and Richard Casaburi. Influence of muscle fiber type and pedal frequency on oxygen uptake kinetics of heavy exercise. *Journal of Applied Physiology*, 81(4):1642–1650, 1996.

[38] R Boushel and CA Piantadosi. Near-infrared spectroscopy for monitoring muscle oxygenation. *Acta Physiologica Scandinavica*, 168(4):615–622, 2000.

[39] Romualdo Belardinelli, Thomas J Barstow, Janos Porszasz, and Karlman Wasserman. Changes in skeletal muscle oxygenation during incremental exercise measured with near infrared spectroscopy. *European journal of applied physiology and occupational physiology*, 70(6):487–492, 1995.

[40] Mireille CP Van Beekvelt, Willy NJM Colier, Ron A Wevers, and Baziel GM Van Engelen. Performance of near-infrared spectroscopy in measuring local o2 consumption and blood flow in skeletal muscle. *Journal of Applied Physiology*, 90(2):511–519, 2001.

[41] Moxy. Moxy muscle oxygenation monitor. `https://www.moxymonitor.com`.

[42] BSXinsight. Bsxinsight cycling edition. `https://www.bsxinsight.com`.

[43] Ralph Beneke. Methodological aspects of maximal lactate steady state—implications for performance testing. *European journal of applied physiology*, 89(1):95–99, 2003.

[44] Véronique L Billat, Pascal Sirvent, Guillaume Py, Jean-Pierre Koralsztein, and Jacques Mercier. The concept of maximal lactate steady state. *Sports medicine*, 33(6):407–426, 2003.

[45] I Jacobs, PA Tesch, Oded Bar-Or, J Karlsson, and R Dotan. Lactate in human skeletal muscle after 10 and 30 s of supramaximal exercise. *Journal of Applied Physiology*, 55(2):365–367, 1983.

[46] Archibald Vivian Hill et al. Muscular movement in man: The factors governing speed and recovery from fatigue. *Muscular Movement in Man: the Factors governing Speed and Recovery from Fatigue.*, 1927.

[47] Hideaki Ishii and Yusuke Nishida. Effect of lactate accumulation during exercise-induced muscle fatigue on the sensorimotor cortex. *Journal of physical therapy science*, 25(12):1637–1642, 2013.

[48] Lennart Jorfeldt, Anders Juhlin-Dannfelt, and J Karlsson. Lactate release in relation to tissue lactate in human skeletal muscle during exercise. *Journal of Applied Physiology*, 44(3):350–352, 1978.

[49] A Nummela, T Vuorimaa, and H Rusko. Changes in force production, blood lactate and emg activity in the 400-m sprint. *Journal of sports sciences*, 10(3):217–228, 1992.

[50] M Aubier, T Trippenbach, and CH Roussos. Respiratory muscle fatigue during cardiogenic shock. *Journal of Applied Physiology*, 51(2):499–508, 1981.

[51] Mark Burnley, Jonathan H Doust, and Anni Vanhatalo. A 3-min all-out test to determine peak oxygen uptake and the maximal steady state. *Medicine & Science in Sports & Exercise*, 38(11):1995–2003, 2006.

[52] Alex Mason, Olga Korostynska, Julien Louis, Luis Eduardo Cordova-Lopez, Badr Abdullah, Jacob Greene, Rob Connell, and John Hopkins. Noninvasive in-situ measurement of blood lactate using microwave sensors. *IEEE Transactions on Biomedical Engineering*, 65(3):698–705, 2018.

[53] Amy S Welch, Angie Hulley, Carrie Ferguson, and Mark R Beauchamp. Affective responses of inactive women to a maximal incremental exercise test: A test of the dual-mode model. *Psychology of Sport and Exercise*, 8(4):401–423, 2007.

[54] Daniel A Keir, Federico Y Fontana, Taylor C Robertson, Juan M Murias, Donald H Paterson, John M Kowalchuk, and Silvia Pogliaghi. Exercise intensity thresholds: Identifying the boundaries of sustainable performance. *Medicine and science in sports and exercise*, 47(9):1932–1940, 2015.

[55] Jamie S Pringle and Andrew M Jones. Maximal lactate steady state, critical power and emg during cycling. *European journal of applied physiology*, 88(3):214–226, 2002.

[56] Jeanne Dekerle, B Baron, L Dupont, J Vanvelcenaher, and P Pelayo. Maximal lactate steady state, respiratory compensation threshold and critical power. *European journal of applied physiology*, 89(3-4):281–288, 2003.

[57] Felipe Mattioni Maturana, Daniel A Keir, Kaitlin M McLay, and Juan M Murias. Can measures of critical power precisely estimate the maximal metabolic steady-state? *Applied Physiology, Nutrition, and Metabolism*, 41(11):1197–1203, 2016.

[58] H Monod and J Scherrer. The work capacity of a synergic muscular group. *Ergonomics*, 8(3):329–338, 1965.

[59] BJ Whipp, DJ Huntsman, TW Storer, N Lamarra, and K Wasserman. A constant which determines the duration of tolerance to high-intensity work. In *Federation proceedings*, volume 41, pages 1591–1591. FEDERATION AMER SOC EXP BIOL 9650 ROCKVILLE PIKE, BETHESDA, MD 20814-3998, 1982.

[60] Anthony J Bull, Terry J Housh, Glen O Johnson, and Sharon R Perry. Effect of mathematical modeling on the estimation of critical power. *Medicine & Science in Sports & Exercise*, 32(2):526, 2000.

[61] Glenn A Gaesser, Tony J Carnevale, Alan Garfinkel, Donald O Walter, and Christopher J Womack. Estimation of critical power with nonlinear and linear models. *Medicine and science in sports and exercise*, 27(10):1430–1438, 1995.

[62] David W Hill. The critical power concept. *Sports medicine*, 16(4):237–254, 1993.

[63] Anni Vanhatalo, Jonathan H Doust, and Mark Burnley. Determination of critical power using a 3-min all-out cycling test. *Medicine and science in sports and exercise*, 39(3):548–555, 2007.

[64] Anni Vanhatalo, Jonathan H Doust, and Mark Burnley. Robustness of a 3 min all-out cycling test to manipulations of power profile and cadence in humans. *Experimental physiology*, 93(3):383–390, 2008.

[65] Tyler M Johnson, Patrick J Sexton, Ashley M Placek, Steven R Murray, and Robert W Pettitt. Reliability analysis of the 3-min all-out exercise test for cycle ergometry. *Medicine and science in sports and exercise*, 43(12):2375–2380, 2011.

[66] Carrie Ferguson, Harry B Rossiter, Brian James Whipp, Andrew J Cathcart, Scott R Murgatroyd, and Susan A Ward. Effect of recovery duration from prior exhaustive exercise on the parameters of the power-duration relationship. *Journal of applied physiology*, 108(4):866–874, 2010.

[67] Phoebe Bickford, Vijay Sarthy M Sreedhara, Gregory M Mocko, Ardalan Vahidi, and Randolph E Hutchison. Modeling the expenditure and recovery of anaerobic work capacity in cycling. In *Multidisciplinary Digital Publishing Institute Proceedings*, volume 2, page 219, 2018.

[68] Philip Friere Skiba, Weerapong Chidnok, Anni Vanhatalo, and Andrew M Jones. Modeling the expenditure and reconstitution of work capacity above critical power. *Medicine and science in sports and exercise*, 44(8):1526, 2012.

[69] Kevin Caen, Jan G Bourgois, Gil Bourgois, K Vermeire, J Boone, et al. The reconstitution of w'depends on both work and recovery characteristics. *Medicine and science in sports and exercise*, 51(8):1745–1751, 2019.

[70] Jason C Bartram, Dominic Thewlis, David T Martin, and Kevin I Norton. Accuracy of w recovery kinetics in high performance cyclists—modeling intermittent work capacity. *International journal of sports physiology and performance*, 13(6):724–728, 2018.

[71] Joel A E Andersson, Joris Gillis, Greg Horn, James B Rawlings, and Moritz Diehl. CasADi – A software framework for nonlinear optimization and optimal control. *Mathematical Programming Computation*, In Press, 2018.

[72] RACERMATE. Computrainer. `https://www.racermateinc.com/computrainer`.

[73] Drew Hartman. Perfpro studio. `https://perfprostudio.com/`.

[74] RC Richard Davison, Jo Corbett, and Les Ansley. Influence of temperature and protocol on the calibration of the computrainer electromagnetically-braked cycling ergometer. *International SportMed Journal*, 10(2):66–76, 2009.

[75] Ida E Clark, Hannah E Gartner, Jade L Williams, and Robert W Pettitt. Validity of the 3-minute all-out exercise test on the computrainer. *The Journal of Strength & Conditioning Research*, 30(3):825–829, 2016.

[76] Bettina Karsten, Simon A Jobson, J Hopker, L Stevens, and C Beedie. Validity and reliability of critical power field testing. *European journal of applied physiology*, 115(1):197–204, 2015.

[77] Garmin. Garmin hear rate sensor. `https://www.garmin.com/en-US/`.

[78] Ida E Clark, Steven R Murray, and Robert W Pettitt. Alternative procedures for the three-minute all-out exercise test. *The Journal of Strength & Conditioning Research*, 27(8):2104–2112, 2013.

[79] R Hugh Morton and L Veronique Billat. The critical power model for intermittent exercise. *European journal of applied physiology*, 91(2-3):303–307, 2004.

[80] O Buttelli, D Seck, H Vandewalle, JC Jouanin, and H Monod. Effect of fatigue on maximal velocity and maximal torque during short exhausting cycling. *European journal of applied physiology and occupational physiology*, 73(1-2):175–179, 1996.

[81] Brian R MacIntosh and Jared R Fletcher. The parabolic power-velocity relationship does apply to fatigued states. *European journal of applied physiology*, 111(2):319, 2011.

[82] Randolph E Hutchison, Faraz Ashtiani, Karlee S Edwards, Gibson A Klapthor, Gregory M Mocko, and Ardalan Vahidi. Effects of w' depletion on the torque-velocity relationship in cycling. *Journal of Strength and Conditioning Research*, 2021.

[83] Arthur Earl Bryson. *Applied optimal control: optimization, estimation and control*. Routledge, 2018.

[84] Richard E Bellman and Stuart E Dreyfus. *Applied dynamic programming*, volume 2050. Princeton university press, 2015.

[85] Marco Belloli, Stefano Giuseppe Giappino, Fabio Cristiano Robustelli, Claudio Somaschini, et al. Drafting effect in cycling: Investigation by wind tunnel tests. In *11th conference of the International Sports Engineering Association, ISEA 2016*, pages 38–43. Elsevier Ltd, 2016.

[86] Nathan Barry, David Burton, John Sheridan, Mark Thompson, and Nicholas AT Brown. Aerodynamic drag interactions between cyclists in a team pursuit. *Sports Engineering*, 18(2):93–103, 2015.

[87] Anil V Rao. A survey of numerical methods for optimal control. *Advances in the Astronautical Sciences*, 135(1):497–528, 2009.

[88] Hans Georg Bock and Karl-Josef Plitt. A multiple shooting algorithm for direct solution of optimal control problems. *IFAC Proceedings Volumes*, 17(2):1603–1608, 1984.

[89] Andreas Wächter and Lorenz T Biegler. On the implementation of an interior-point filter line-search algorithm for large-scale nonlinear programming. *Mathematical programming*, 106(1):25–57, 2006.

[90] Pierre Bonami, Lorenz T Biegler, Andrew R Conn, Gérard Cornuéjols, Ignacio E Grossmann, Carl D Laird, Jon Lee, Andrea Lodi, François Margot, Nicolas Sawaya, et al. An algorithmic framework for convex mixed integer nonlinear programs. *Discrete Optimization*, 5(2):186–204, 2008.

[91] Ailsa H Land and Alison G Doig. An automatic method for solving discrete programming problems. In *50 Years of Integer Programming 1958-2008*, pages 105–132. Springer, 2010.